Journal Pre-proofs

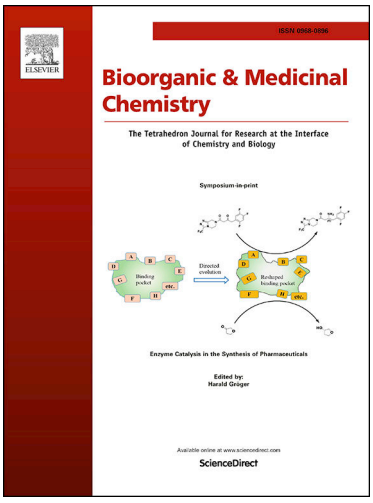

N-Hydroxyformamide LpxC inhibitors, their *in vivo* efficacy in a mouse *Escherichia coli* infection model, and their safety in a rat hemodynamic assay

Takeru Furuya, Adam B. Shapiro, Janelle Comita-Prevoir, Eric J. Kuenstner, Jing Zhang, Seth D. Ribe, April Chen, Daniel Hines, Samir H. Moussa, Nicole M. Carter, Mark A. Sylvester, Jan A. C. Romero, Camilo V. Vega, Michael D. Sacco, Yu Chen, John P. O'Donnell, Thomas F. Durand-Reville, Alita A. Miller, Ruben A. Tommasi

PII: S0968-0896(20)30656-8
DOI: https://doi.org/10.1016/j.bmc.2020.115826
Reference: BMC 115826

To appear in: *Bioorganic & Medicinal Chemistry*

Received Date: 29 September 2020
Accepted Date: 22 October 2020

Please cite this article as: T. Furuya, A.B. Shapiro, J. Comita-Prevoir, E.J. Kuenstner, J. Zhang, S.D. Ribe, A. Chen, D. Hines, S.H. Moussa, N.M. Carter, M.A. Sylvester, J. A. C. Romero, C.V. Vega, M.D. Sacco, Y. Chen, J.P. O'Donnell, T.F. Durand-Reville, A.A. Miller, R.A. Tommasi, *N*-Hydroxyformamide LpxC inhibitors, their *in vivo* efficacy in a mouse *Escherichia coli* infection model, and their safety in a rat hemodynamic assay, *Bioorganic & Medicinal Chemistry* (2020), doi: https://doi.org/10.1016/j.bmc.2020.115826

N-Hydroxyformamide LpxC inhibitors, their *in vivo* efficacy in a mouse *Escherichia coli* infection model, and their safety in a rat hemodynamic assay

Takeru Furuya[a,*], Adam B. Shapiro[a], Janelle Comita-Prevoir[a], Eric J. Kuenstner[a], Jing Zhang[a], Seth D. Ribe[a], April Chen[a], Daniel Hines[a], Samir H. Moussa[a], Nicole M. Carter[a], Mark A. Sylvester[a], Jan A. C. Romero[a], Camilo V. Vega[a], Michael D. Sacco[b], Yu Chen[b], John P. O'Donnell[a], Thomas F. Durand-Reville[a], Alita A. Miller[a], Ruben A. Tommasi[a,*]

[a] Entasis Therapeutics, 35 Gatehouse Dr., Waltham MA 02451, USA

[b] Department of Molecular Medicine, Morsani College of Medicine, University of South Florida 12901 Bruce B. Downs Blvd, MDC 07, Tampa, FL 33612 USA

* Corresponding authors

ARTICLE INFO

Keywords:

LpxC, antibacterial, *Escherichia coli, Klebsiella pneumonia, Pseudomonas aeruginosa*

ABSTRACT

UDP-3-*O*-(*R*-3-hydroxyacyl)-*N*-acetylglucosamine deacetylase (LpxC), the zinc metalloenzyme catalyzing the first committed step of lipid A biosynthesis in Gram-negative bacteria, has been a target for antibacterial drug discovery for many years. All inhibitor chemotypes reaching an advanced preclinical stage and clinical phase 1 have contained terminal hydroxamic acid, and

none have been successfully advanced due, in part, to safety concerns, including hemodynamic effects. We hypothesized that the safety of LpxC inhibitors could be improved by replacing the terminal hydroxamic acid with a different zinc-binding group. After choosing an *N*-hydroxyformamide zinc-binding group, we investigated the structure-activity relationship of each part of the inhibitor scaffold with respect to *Pseudomonas aeruginosa* and *Escherichia coli* LpxC binding affinity, *in vitro* antibacterial potency and pharmacological properties. We identified a novel, potency-enhancing hydrophobic binding interaction for an LpxC inhibitor. We demonstrated *in vivo* efficacy of one compound in a neutropenic mouse *E. coli* infection model. Another compound was tested in a rat hemodynamic assay and was found to have a hypotensive effect. This result demonstrated that replacing the terminal hydroxamic acid with a different zinc-binding group was insufficient to avoid this previously recognized safety issue with LpxC inhibitors.

1. Introduction

The existential threat of antibiotic resistance necessitates the development of new antibiotics with novel mechanisms of action.[1] Several of the WHO priority pathogens are Gram negative bacteria. They present a challenge for the discovery of new antibacterial drugs owing, in part, to their outer membrane permeability barrier. However, the unique biochemical machinery involved in biosynthesis of the outer membrane presents targets for Gram negative-selective antibiotics. One such target is UDP-3-*O*-(*R*-3-hydroxyacyl)-*N*-acetylglucosamine deacetylase (LpxC), the zinc-containing deacetylase enzyme responsible for the first committed step of lipid A biosynthesis (Scheme 1).[2] As the anchor for lipopolysaccharide, which is itself indispensable in most Gram-negative bacteria, lipid A is thus required for proper outer membrane assembly and function. Inhibition of LpxC function is lethal to most Gram-negative pathogens, and in other cases results in a permeable membrane that enhances susceptibility to other antibiotics.[3] The importance of lipid A biosynthesis, coupled with a lack of homologous mammalian enzymes, has inspired numerous drug discovery campaigns aimed towards the development of LpxC inhibitors.[4-11]

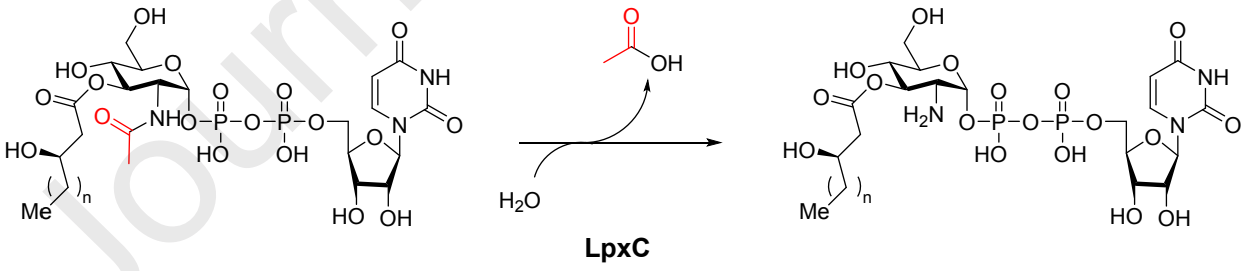

Scheme 1. The deacetylation reaction catalyzed by LpxC (*E. coli*: n = 10, *P. aeruginosa*: n = 6)

Although LpxC inhibitors have been explored since the mid-1990s,[12] a drug has yet to advance beyond phase 1 clinical trials. Most prominently, the development of ACHN-975 (**1**) was discontinued after a phase 1 trial, owing to local inflammation at the injection site.[13] A trial involving RC-01, another LpxC inhibitor, was recently terminated, also for safety reasons.[14] Notably, all the LpxC inhibitors that advanced to late-stage development contained terminal hydroxamic acids (Fig. 1). Achaogen subsequently demonstrated that both the terminal hydroxamic acid **1**, and the dehydroxylated amide metabolite **1a** were responsible for hypotension-related cardiovascular toxicity.[15] In addition, hydroxamic acids pose a multitude of potential off-target effects and broader toxicity issues. Examples include inhibition of metalloenzymes (e.g. matrix metalloproteinases (MMP)[16] and histone deacetylases (HDAC)[17]), liberation of toxic hydroxylamine via carbonyl hydrolysis, and production of highly reactive and mutagenic isocyanates via physiologically relevant Lossen rearrangements[18]. Therefore, we sought to identify an LpxC inhibitor series with a safer alternative zinc-binding warhead.

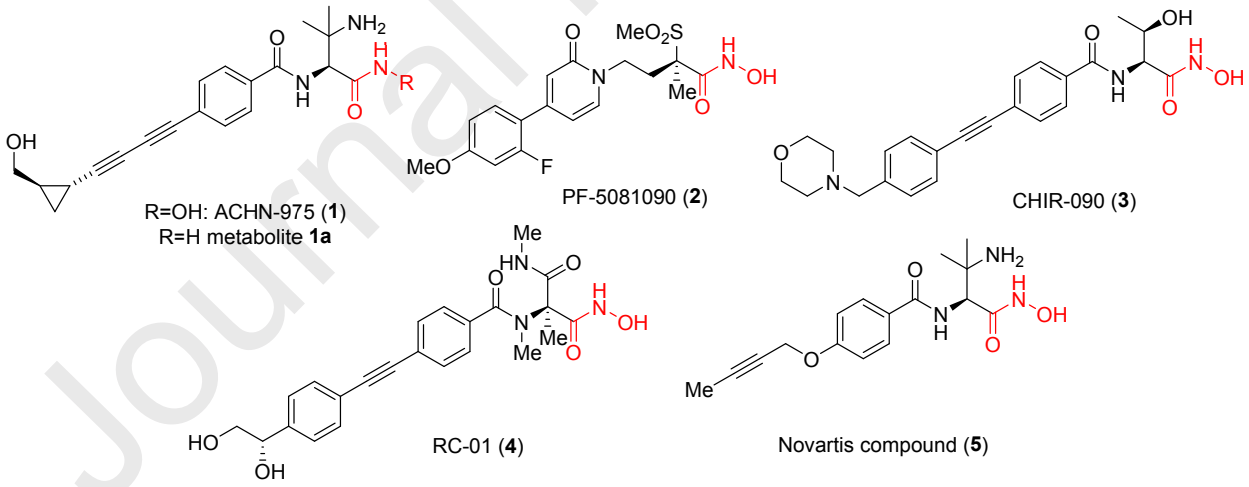

Fig. 1. Representative structures of known LpxC inhibitors

2. Results and discussion

2.1. Chemistry

Scheme 2 depicts the syntheses of lead compounds **19** and **20** used in the efficacy and safety studies, respectively. The route was designed to have three key intermediates: THP-protected *N*-hydroxyformamide **7**, alkyne **10**, and benzotriazole aldehyde **14**. Their late stage assembly provided a convergent and modular synthesis, thereby enabling an efficient study of structure-activity-relationships (SAR). The THP-protected *N*-hydroxyformamide **7** was synthesized in a single step from commercially available amine **6** with 1,1-carbonyldiimidazole (CDI) and formic acid. The alkyne **10** used in the Sonogashira reaction for the synthesis of **20** was prepared in two steps from commercially available 2-thia-6-azaspiro[3.3]heptane (**8**). Preparation of 4-(morpholinomethyl)phenylacetylene used in the synthesis of **19** was previously described in the literature.[19]

The commercially available 1-fluoro-4-iodo-2-nitrobenzene (**11**) was first converted to diamine **12** by nucleophilic aromatic substitution with 2,2-diethoxyethan-1-amine, which was then followed by reduction of the nitro group with zinc/NH_4Cl. Diazotization of the resulting diamine **12** was accompanied by cyclization to install the benzotriazole core in compound **13**. After deprotection of the diethylacetal moiety with aqueous HCl, the resulting aldehyde **14** was treated with the trimethylsilylimidate generated by the combination of **7**, TMSCl, and Et_3N. The TMS-protected acyl aminal **15** thus obtained served as an important synthetic intermediate in our synthesis. While rare, such structures have previously been described in the literature.[20, 21]

In the endgame of the synthesis, displacement of the silyloxy group with sodium thiomethoxide in the presence of TMSOTf also resulted in concomitant deprotection of the *N*-hydroxyformamide. Fragment unification via the Sonogashira coupling was followed by chiral HPLC separation to complete the syntheses of targets **19** and **20**.

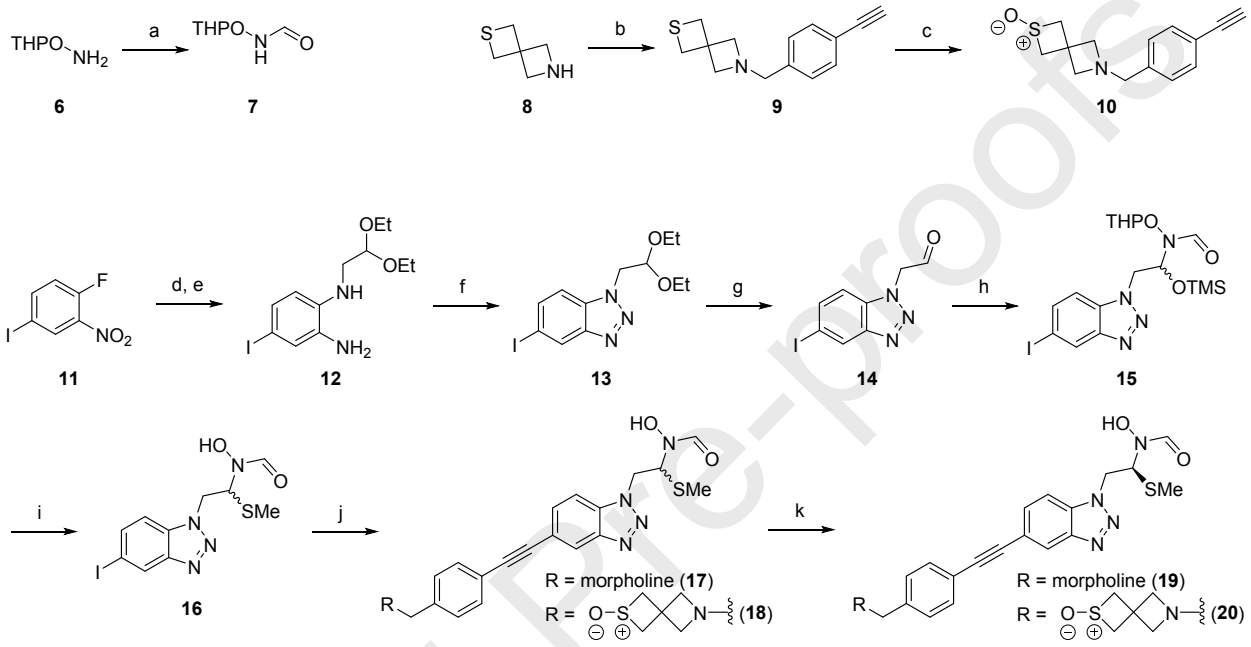

Scheme 2. Reagents and conditions: (a) CDI, formic acid, Et_3N, CH_2Cl_2, 80%; (b) 4-ethynylbenzaldehyde, $NaBH(OAc)_3$, THF, 84%; (c) $NaIO_4$, MeOH, 81%; (d) 2,2-diethoxyethan-1-amine, $^iPr_2NEt$, MeCN; (e) Zn, NH_4Cl, H_2O, THF, 87% (2 steps); (f) $NaNO_2$, AcOH, H_2O, toluene, 61%; (g) HCl, H_2O (h) **7**, TMSCl, Et_3N, toluene, 50% (2 steps); (i) TMSOTf, NaSMe, CH_2Cl_2, 87%; (j) **10** or 4-(morpholinomethyl)phenylacetylene, CuI, $Pd(PPh_3)_4$, Et_3N, NMP, 46% (**17**), 40% (**18**); (k) chiral HPLC separation, 28% (**19**), 34% (**20**)

2.2. Strategy and hit identification

Key interactions in the LpxC enzyme binding pocket have been well-characterized.[9] As shown for *P.aeruginosa* LpxC bound to CHIR-090 (**3**) (Fig. 2),[9] the defining elements of the binding pocket include: 1) bidentate chelation of the warhead to a zinc ion, 2) polar interactions in and

around the ribose sugar-binding pocket (sugar pocket), 3) hydrophobic interactions with the lipophilic tunnel region, and 4) the presence of a solvent-exposed region at the exit of the lipophilic tunnel.

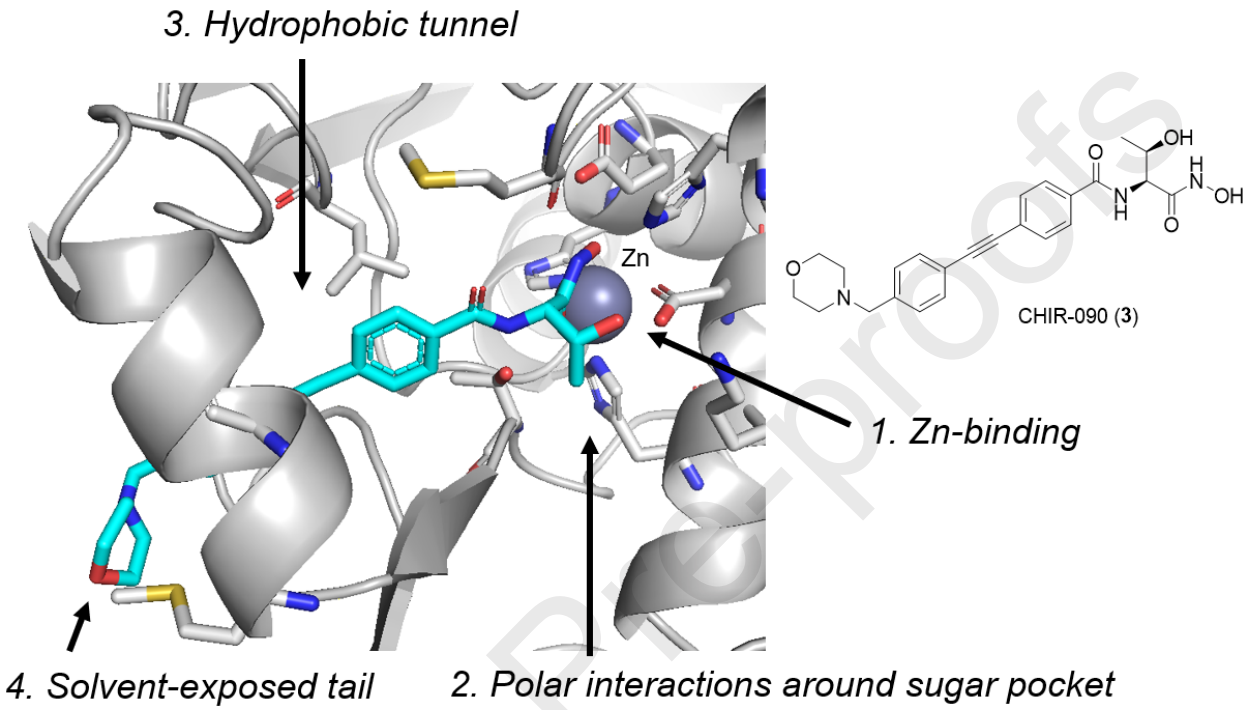

Fig. 2. Key interactions in the LpxC enzyme binding pocket observed in *P. aeruginosa* LpxC−CHIR-090 (**3**) co-crystal structure (PDB code: 5VWM)

We first implemented a docking model using the ICM-Pro software (Molsoft) based on the available co-crystal structures of *P. aeruginosa* LpxC. A virtual screen with several commercially available fragment libraries gave a few non-terminal-hydroxamic-acid hits (data not shown). A subsequent hit-to-lead campaign identified *N*-hydroxyformamide (NHF) as the most promising warhead. However, all previous LpxC inhibitors that reached late-stage preclinical development (Fig. 1) contain a heteroatom α to the hydroxamic acid carbonyl group

(Scheme 3). This prevented us from simply replacing the terminal hydroxamic acid warhead with *N*-hydroxyformamide, as this would lead to the potentially unstable aminal-type structure **21** (Scheme 3A). Therefore, our initial lead optimization focused on the identification of an appropriate linker between the NHF warhead and the hydrophobic core (X−Y) shown in the general structure **22** (Scheme 3B).

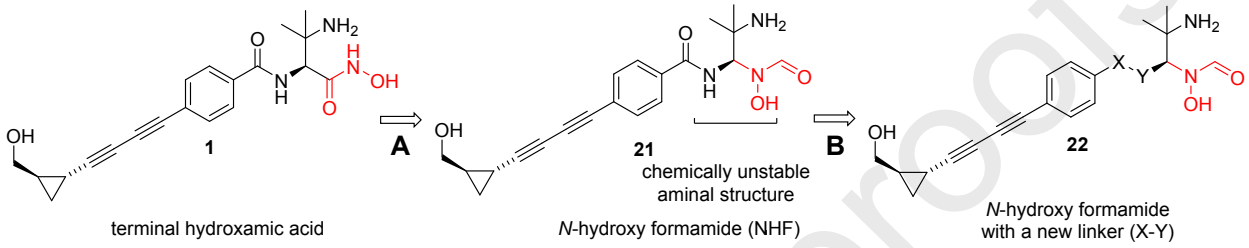

Scheme 3. Strategy for incorporating *N*-hydroxyformamide

2.3. Lead optimization towards an in vivo efficacy study

We used CHIR-090 (**3**) as the starting scaffold to explore the NHF warhead. As expected, the compound with an alkyl chain linker without a polar functional group α to the warhead (compound **23**) showed much lower enzymatic and *in vitro* antibacterial potency than CHIR-090 (Table 1). The popularity of the benzamide core in the known LpxC inhibitors (compounds **1**,**3**,**4**, and **5** in Fig. 1) was attributed in the literature to the hydrogen bond between the amide NH and a threonine residue (T190, *P. aeruginosa* LpxC), as well as its preferred *s*-cis geometry.[22] Thus, we investigated fused heterocyclic bicyclic cores (HetAr) to increase the rigidity and reduce the entropic penalty associated with proper ligand orientation. Heteroatoms were incorporated to improve the poor antibacterial potency seen in **23**. A 6,5-fused ring system improved *in vitro* antibacterial potency, but the placement of heteroatoms at the right positions was crucial to

obtain the optimal result (Table 1). Benzotriazole **24g** was selected as the basis for further optimization, with an MIC of 4 mg/L against *E. coli* (ATCC 25922) and IC_{50} values of 44 nM and 20 nM against *P. aeruginosa* and *E. coli* LpxC, respectively.

Table 1. Optimization of the heterocyclic core

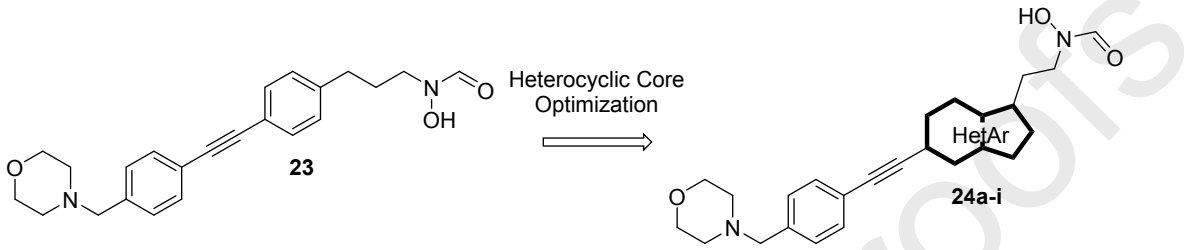

23 **24a-i**

Compound	HetAr	*P.a.*[a] IC_{50} (μM)	*E.c.*[b] IC_{50} (μM)	*E.c.* (ATCC 25922) MIC[c] (mg/L)
CHIR-090 (**3**)	N/A	<0.001	<0.010	0.13
23	N/A	0.063	0.021	32
24a	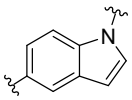	0.045	0.010	2
24b	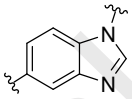	1.1	0.082	16
24c	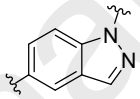	0.064	0.028	4
24d	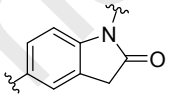	0.17	0.025	4
24e	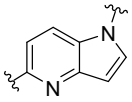	1.0	0.17	32
24f	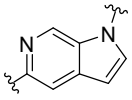	1.0	0.74	64
24g	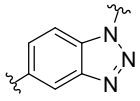	0.044	0.020	4

24h	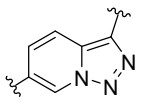	0.037	0.015	4
24i	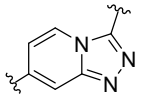	0.28	0.054	16

[a] *Pseudomonas aeruginosa;* [b] *Escherichia coli;* [c] minimal inhibitory concentration

We next focused on optimization of the position α to the NHF warhead. The recognition that hydrophilic substituents at analogous positions in previous campaigns interacted with the sugar pocket created by polar amino acids such as lysine (K238) and histidine (H264) led to the supposition that similar results could be obtained with our chemotype (residue numbers are from *P. aeruginosa* LpxC). Contrary to our expectations, introduction of a hydroxymethyl substituent (**25a**, Table 2) did not improve potency, while small alkyl and heteroalkyl groups (e.g. **25c** and **17**) led to >10-fold improvement in enzyme binding potency. Alkoxy groups were promising (**25e** and **25f**) but showed lower chemical stability (data not shown). Chiral separation of **17** demonstrated substantially higher activity of the *S* enantiomer compared to the *R* enantiomer (**25g** vs **19**).

Table 2. Optimization of the α-position

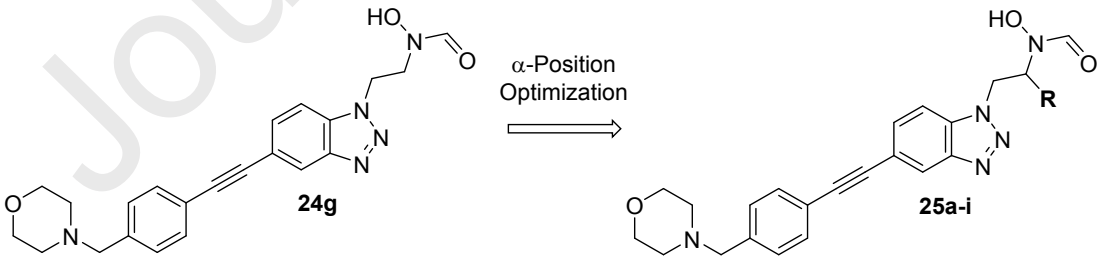

Compound	R	*P.a.*[a] IC_{50} (nM)	*E.c.*[b] IC_{50} (nM)	*E.c.* (ATCC 25922) MIC (mg/L)
24g	H	44	20	2
25a	CH_2OH	61	42	2
25b	Me	14	14	2
25c	Et	2.4	<10	1
17	SMe	1.3	<10	0.25
25d	SEt	5.4	<10	0.5
25e	OMe	7.3	<10	0.25
25f	OEt	41	22	2
19	(*S*)-SMe	<1	<10	0.13
25g	(*R*)-SMe	21	41	4

[a] *Pseudomonas aeruginosa;* [b] *Escherichia coli*

The crystal structure of **19** with *P. aeruginosa* LpxC revealed an unexpected binding mode, consistent with the structure-activity relationship (SAR), in which there were no polar interactions between the α-substituent and the sugar pocket (Fig. 3). Rather, the thiomethyl group of **19** occupied the hydrophobic dent created by Leu-18, Ile-102, and Thr-75. Overlay of our co-crystal structure with that of CHIR-090 (**3**) showed that the binding geometries were nearly identical from the morpholine tail to the warhead β position, at which point they diverged in their pathways towards the zinc ion. This result was encouraging because **19** achieved high potency without exploiting the binding interactions in and around the sugar pocket. The CHIR-090 (**3**) analog that does not possess an α substituent (**26**) was synthesized to compare our lead series with others in a similar development stage (Table 3A). While both **19** and **26** lack functional groups that are capable of interaction with the sugar pocket, our series demonstrated higher enzymatic and antibacterial potency. If binding interactions in and around the sugar

pocket conferred a similar benefit to our scaffold, our lead series could achieve much higher antibacterial potency than any previously developed scaffold.

To investigate the hypothesis that our scaffold could be further improved by an appropriate β-substituent to interact with the sugar pocket, we synthesized **27a** and **27b** (Table 3B). Indazole and ethyl groups were used in place of benzotriazole and thiomethyl groups in **19** for the sake of operationally simpler syntheses. In **27b**, a hydroxypropyl group was introduced at the β-position, which was intended to mimic the hydroxyethyl group in CHIR-090 (**3**). Though **27b** is a 1:1 mixture of diastereomers at the secondary alcohol, it exhibited four-fold improvement in both enzymatic and antibacterial potency, thereby demonstrating that our scaffold could be further optimized with an appropriate β-substituent.

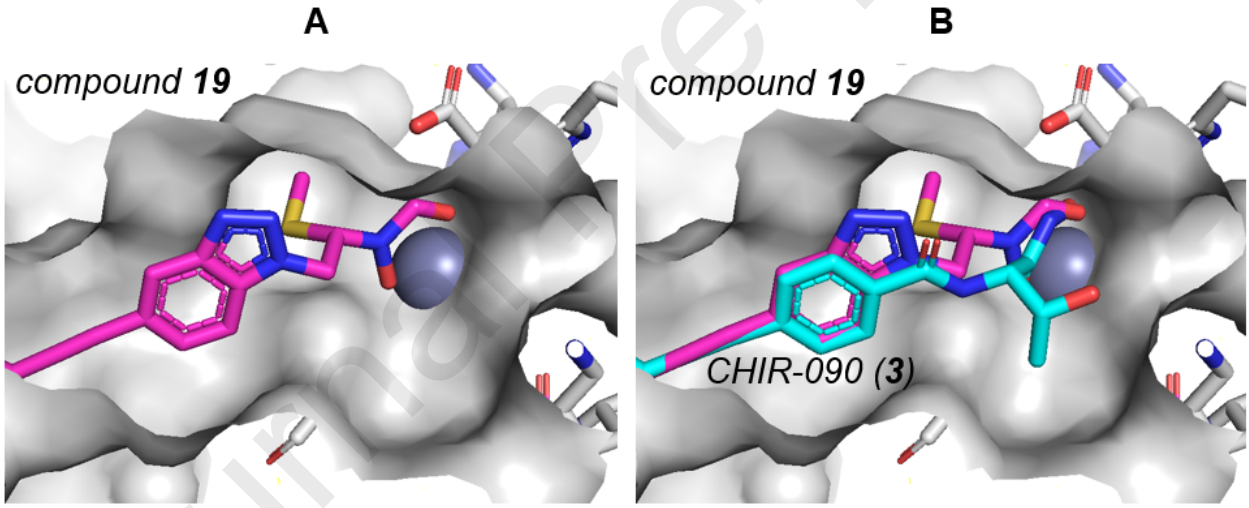

Fig. 3. X-ray crystallographic analysis of **19** (PDB code: 7K99) compared with CHIR-090 (**3**). (**A)** Crystal structure of **19**; (**B**) Overlay of **19** and **3**

Table 3. Effect of substituents for the sugar pocket binding. (**A**) Comparison of **19** with a compound with the same lead optimization stage; (**B**) Model compounds for investigating the effect of a β-substituent

A:

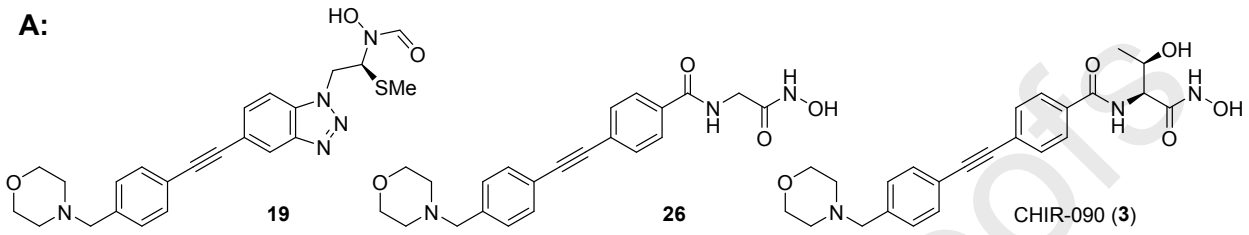

B:

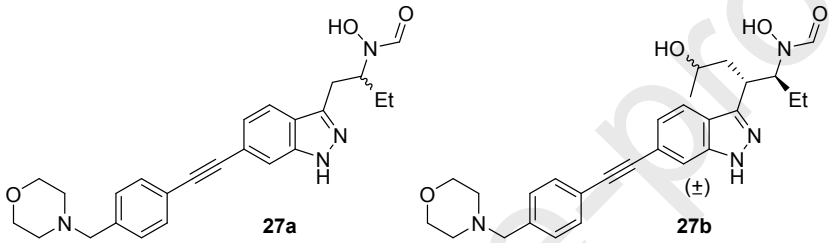

Compound	*P.a.*[a] IC_{50} (nM)	*E.c.*[b] IC_{50} (nM)	*P.a.* (PAO1) MIC (mg/L)	*E.c.* (ATCC 25922) MIC (mg/L)	*K.p.*[c] (ATCC 700603) MIC (mg/L)
19	<1	<10	4	0.13	4
26	63	21	64	16	>64
3	<1	<10	1	0.13	2
27a	10	19	>64	4	>64
27b	2.5	<10	16	1	32

[a] *Pseudomonas aeruginosa;* [b] *Escherichia coli;* [c] *Klebsiella pneumoniae*

2.4. Evaluation of in vivo efficacy

We next sought to investigate the *in vivo* efficacy of **19** in a neutropenic mouse thigh infection model with *E. coli* ARC6599 (MIC = 0.03 mg/L). The compound demonstrated dose-dependent *in vivo* efficacy by achieving a 2 $\log_{10}$ reduction in CFU count after 24 hours with a 200 mg/kg

(s.c.) QD dose and >3.2 log_{10} reduction (to below the limit of detection) with a 200 mg/kg (s.c.) BID dose (Fig. 4). The pharmacokinetic parameters are summarized in Table 4.

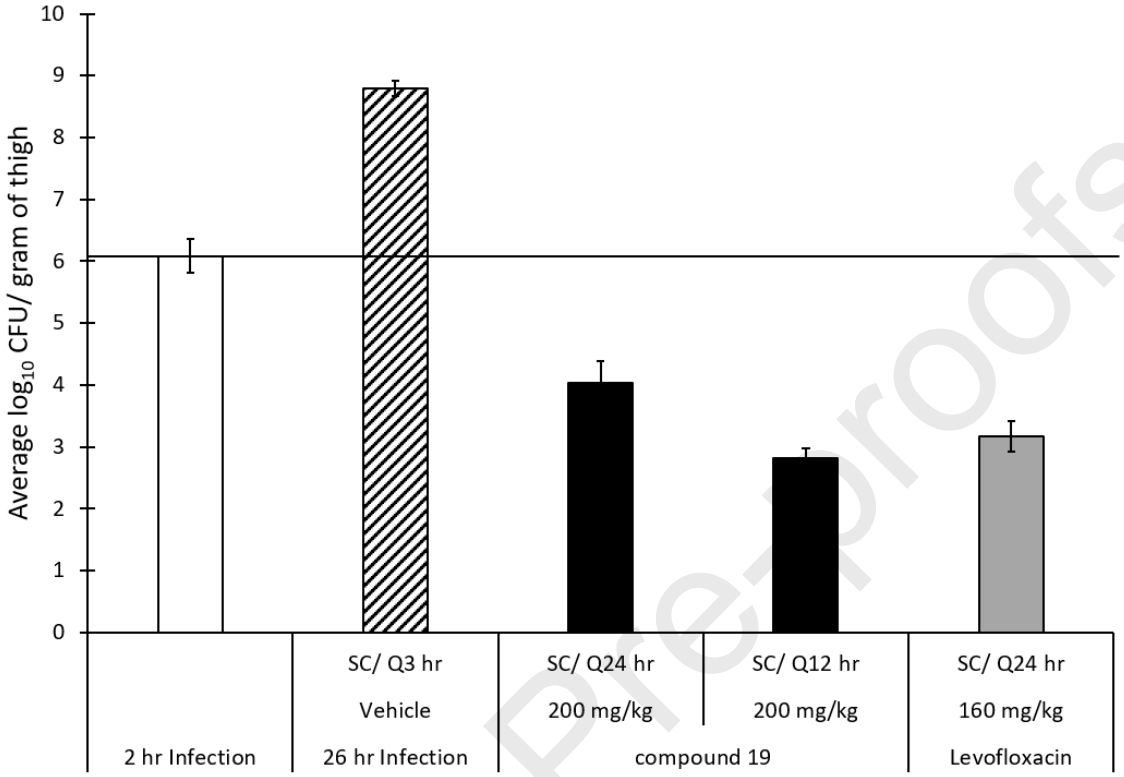

Fig. 4. Demonstration of *in vivo* efficacy by a neutropenic mouse thigh infection model

Table 4. Pharmacokinetics parameters of **19**

Dose (mg/kg)	route	C_{max}[a] (mg/mL)	AUC[b] (hr*mg/mL)	CL_{obs}[c] (L/hr/kg)	V_d[d] (L/kg)	*f*AUC[e]/MIC	mouse PPB[f] (%free)
200	s.c.	21.5	34.8	4.8	10.1	104	9

[a] maximum plasma concentration; [b] area under the curve; [c] observed clearance; [d] volume of distribution; [e] area under the unbound drug concentration-time curve; [f] plasma protein binding

After the demonstration of the *in vivo* efficacy of **19**, we shifted focus to the physicochemical, drug metabolism and pharmacokinetics (DMPK), and secondary pharmacology profile of our series. We planned to evaluate the key cardiovascular toxicity and projected therapeutic window using a rat hemodynamic assay.[15] In order to achieve this, high exposure was necessary to properly evaluate the maximum tolerated concentration. Compound **19** unfortunately suffered from poor physicochemical properties and an undesirable DMPK profile consisting of high plasma protein binding, high hepatic clearance, and low aqueous solubility. Moreover, compound **19** demonstrated acetylcholinesterase (AChE) enzyme inhibition at a relatively low concentration (3.5 μM) in the secondary pharmacology panel (data not shown). Therefore, we decided to further optimize the lead structure **19** by modifying the morpholine tail. Because the morpholine moiety in **19** is exposed to solvent by its placement outside the hydrophobic tunnel in the crystal structure (Fig. 2), we anticipated its modification would not dramatically affect enzymatic potency, while allowing us to modulate physicochemical and DMPK characteristics.

2.5. Lead optimization towards cardiovascular safety study

Akin to the extensive optimization efforts on the tail moiety described elsewhere,[10] our scaffold benefited from tail optimization (Table 5). The morpholine tail in **19** was replaced by known morpholine bioisosteres and structurally related heterocycles. Among the many different tails investigated, spiro-azetidine-thiatane-oxide (**20**) stood out in terms of lower rat plasma protein binding (9% unbound, compared to 3% for **19**) and weaker AChE inhibition (>100 μM, compared to 3.5 μM for **19**). In addition, a trifluoroacetate salt of **20** exhibited high solubility in

A5D (2.5% dextrose in 20 mM acetate buffer, pH 5) (>200 mg/mL) and had an acceptable rat PK profile (CL = 2.0 L/hr/kg and V_{ss} = 0.58 L/kg when dosed at 90 mg/kg iv), allowing us to advance **20** to the rat hemodynamic cardiovascular safety study.

Table 5. Optimization of the morpholine tail

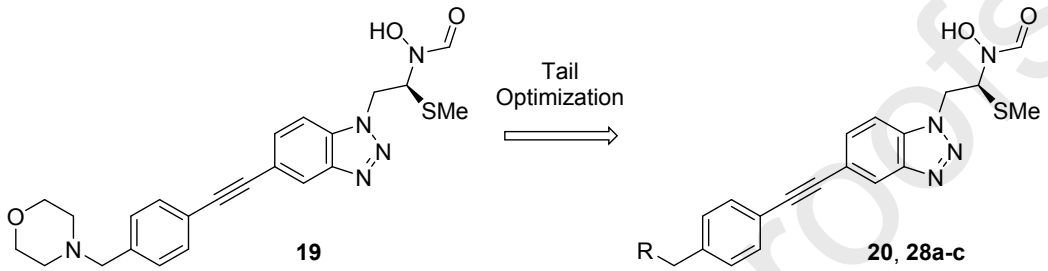

Compound	R	*P.a.*[a] IC_{50} (nM)	*E.c.*[b] IC_{50} (nM)	*P.a.* (PAO1) MIC (mg/L)	*E.c.* (ATCC 25922) MIC (mg/L)	*K.p.*[c] (ATCC 700603) MIC (mg/L)	AChE IC_{50} (μM)	PPB mouse/rat (%free)
19	morpholine	<1	<10	4	0.13	4	3.5	9/3
28a	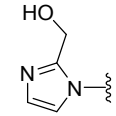	<1	<10	2	0.25	2	15	5/3
28b		<1	<10	4	0.13	4	32	10/6
20	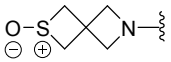	<1	<10	4	0.25	8	>100	9/9
28c	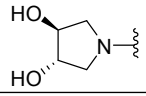	<1	<10	2	0.5	8	22	9/6

[a] *Pseudomonas aeruginosa;* [b] *Escherichia coli;* [c] *Klebsiella pneumoniae*

2.6. Evaluation of safety with rat hemodynamic assay

Systolic blood pressure and drug plasma concentration were measured in adult male Sprague-Dawley rats while the test article was continuously infused intravenously. Following a period of equilibration, rats received A5D vehicle for 30 min, followed by 500 mg/kg/hr of **20** or vehicle for 60 min, followed by 30 min of vehicle to monitor reversibility of any hypotensive effect. Fig. 5 shows the results of this hemodynamic assay. Unlike rats receiving the vehicle, rats receiving **20** showed hypotension with plasma concentrations of **20** between 11 and 16 μg/mL, and a lack of rebound in the recovery phase. Albeit generated from a small study with significant variability, we believe that the data refute our hypothesis that the replacement of the terminal hydroxamic acid warhead would significantly reduce the safety risk. It is likely that the toxicities associated with LpxC inhibitors are driven by the entire pharmacophore, rather than just the terminal hydroxamic acid. For example, basic amines in close proximity to aromatic rings are a common ion channel pharmacophore.[23] Given the requirement for a hydrophobic core flanked with a polar zinc-binding group, it seems inevitable that some off-target toxicities will be encountered in this chemical space. To date, well-defined biological targets responsible for the toxicities of LpxC inhibitors have yet to be elucidated. Without this information, risk management prior to candidate nomination remains a monumental task.

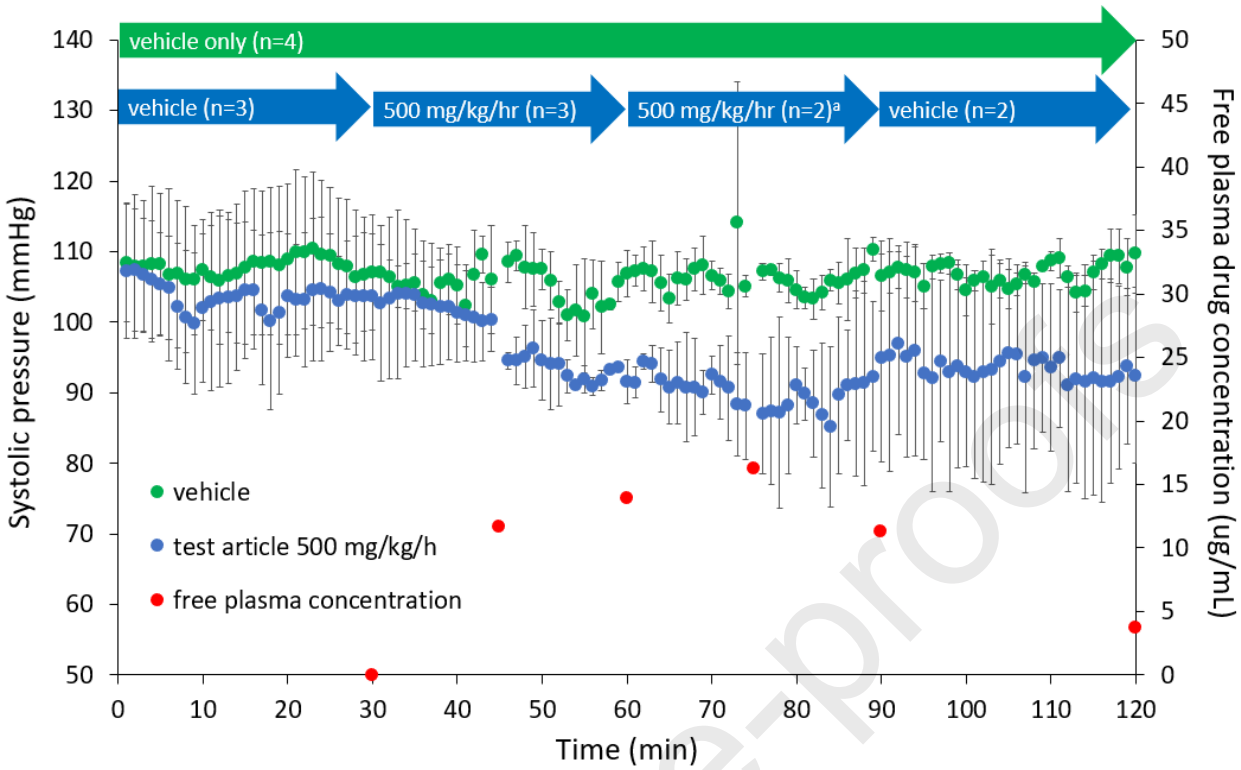

Fig. 5. Evaluation of cardiovascular safety of **20** by rat hemodynamic assay

[a] Initially, a higher dose (1000 mg/kg/hr) was infused between 60−90 min, but the animal expired at the end of the 30 min infusion. Thus, 500 mg/kg/hr dose was used for the rest of the study between 60−90 min.

3. Conclusions

The focus of our medicinal chemistry campaign was the hypothesis that an *N*-hydroxyformamide warhead could overcome previous toxicity issues with LpxC inhibitors by replacing the terminal hydroxamic acid. We developed a potent and efficacious series of LpxC inhibitors for Gram-negative bacterial infections by unprecedented exploitation of a unique binding pocket. The series has the potential to be further improved by exploiting interactions in and around the sugar pocket. Unfortunately, despite acceptable PK and *in vitro* safety data, a compound from the

series showed an unacceptable hypotensive effect in a rat study. Our efforts thus serve to highlight the difficulty of safely targeting LpxC in antibacterial drug development.

4. Experimental

4.1. Chemistry

4.1.1. General information

All solvents and reagents used were obtained commercially and used as received unless noted otherwise. ^{1}H and ^{13}C NMR spectra were recorded at 300 K using a Brucker Ultrashield 300 or 400 MHz instrument. Chemical shifts are reported as parts per million relative to tetramethylsilane (TMS) (0.00) for ^{1}H and ^{13}C NMR. Silica gel chromatographies were performed on ISCO Combiflash Companion or Rf 200 Instruments using ISCO RediSep Flash Cartridges (particle size: 35−70 microns) or Silicycle SilicaSep Flash Cartridges (particle size: 40−63 microns). Reverse phase chromatography was performed on ISCO Combiflash Rf 200 Instruments using RediSep High Performance Gold C18 and C18Aq columns. Preparative reverse phase HPLC was carried out using a Gilson instrument. When not indicated, compound intermediates and reagents were purchased from chemical supply houses. All electrospray ionization mass spectra (ESI-MS) were recorded via reverse phase UPLC-MS with a Waters Acquity UPLC instrument with diode array and electrospray ionization detectors, a UPLC HSS T3, 2.1 × 30 mm, 1.8 μm column and a gradient of 2 to 98% acetonitrile in water with 0.1% formic acid over 2.0 minutes at 1 mL/min. Injection volume was 1 μL and the column temperature was 30 ºC. Detection was based on electrospray ionization (ESI) in positive and

negative polarity using Waters ZQ mass spectrometer (Milford, MA, USA), diode array UV detector from 210 to 400 nm, and evaporative light scattering detector (Cedex 75, Sedere, Alfortville, France).

The general synthetic route illustrated in Scheme 2 was used to make compounds **24a**−**i**. For some compounds, the corresponding halogen-substituted heterocycles were commercially available, which were alkylated with 2-bromoethanol or bromoacetaldehyde diethyl acetal to prepare intermediates similar to **14**. For other compounds, the heterocyclic cores were assembled following reported procedures.[24,25] For compounds **25a**−**g**, a differently substituted aminoalcohol or alcohol was used in place of 2,2-diethoxyethan-1-amine or sodium thiomethoxide, respectively, followed by a similar reaction sequence. Compound **26** was synthesized following the procedure reported for the synthesis of CHIR-090 (**3**),[26] except a glycin-derived warhead piece was used in place of the threonine-drived one. Synthesis of compounds **27b** is shown in Supplementary Material. Compound **27a** was synthesized in a similar manner as **27b**. Compounds **28a**−**c** and **29** were synthesized following the route depicted in Scheme 2, except a differently substituted alkyne was used for the Sonogashira reaction.

4.1.2. N-tetrahydropyran-2-yloxyformamide (7)

Under nitrogen, to a stirred solution of CDI (8.1 g, 50 mmol. 1.0 equiv) in CH_2Cl_2 (200 mL) at 23 ºC was added formic acid (1.9 mL, 50 mmol, 1.0 equiv). After stirring for 10 min at 23 ºC, *O*-tetrahydropyran-2-ylhydroxylamine (**6**) (5.9 g, 50 mmol, 1.0 equiv) was added to the reaction mixture in one portion, followed by dropwise addition of Et_3N (7.0 mL, 50 mmol, 1.0 equiv). After stirring for 20 min at 23 ºC, the reaction mixture was concentrated and the residue was

purified with chromatography on silica gel eluting with hexanes/EtOAc to afford *N*-tetrahydropyran-2-yloxyformamide (**7**) (7.3 g, 80% yield). ^{1}H NMR (300 MHz, $CDCl_3$, 23 ºC) δ: 8.60–7.99 (m, 2H), 5.04–4.88 (m, 1H), 4.02–3.78 (m, 1H), 3.65–3.53 (m, 1H), 1.99–1.48 (m, 6H).

*4.1.3. 6-[(4-ethynylphenyl)methyl]-2-thia-6-azaspiro[3.3]heptane (**9**)*

Under nitrogen, to a stirred solution of 2-thia-6-azaspiro[3.3]heptane oxalic acid salt (**8**) (970 mg, 4.73 mmol. 1.30 equiv) in THF (24 mL) at 23 ºC was added triethylamine (0.659 mL, 4.73 mmol. 1.30 equiv). After stirring for 20 min at 23 ºC, 4-ethynylbenzaldehyde (472 mg, 3.63 mmol, 1.00 equiv) and $NaBH(OAc)_3$ (1.28 g, 6.05 mmol, 1.67 equiv) were added to the reaction mixture at 0 ºC. After stirring for 3 hr at 23 ºC, water/ice was added to the reaction mixture. The resulting mixture was extracted with EtOAc. The combined organic layers were washed with brine and dried over $MgSO_4$. The filtrate was concentrated in vacuo and the residue was purified with chromatography on a C18Aq column eluting with MeCN/H_2O to afford 6-[(4-ethynylphenyl)methyl]-2-thia-6-azaspiro[3.3]heptane (**9**) (700 mg, 84% yield). MS: [M+H] = 230.1 ($C_{14}H_{15}NS$).

*4.1.4. 6-[(4-ethynylphenyl)methyl]-2lambda4-thia-6-azaspiro[3.3]heptan-2- one (**10**)*

Under air, to a stirred solution of 6-[(4-ethynylphenyl)methyl]-2-thia-6-azaspiro[3.3]heptane (**9**) (111 mg, 0.484 mmol, 1.00 equiv) in MeOH (2.4 mL) at 0 ºC was added a solution of $NaIO_4$ (104 mg, 0.484 mmol, 1.00 equiv) in water (2.4 mL) dropwise. After stirring for 1 hr at 0 ºC, the reaction mixture was warmed to 23 ºC and further stirred for 1 hr. The reaction mixture was

diluted with CH_2Cl_2 and the layers were separated. The organic layer was washed with brine and dried over Na_2SO_4. The filtrate was concentrated in vacuo and the residue was purified with chromatography on a C18Aq column eluting with MeCN/H_2O to 6-[(4-ethynylphenyl)methyl]-2lambda4-thia-6-azaspiro[3.3]heptan-2- one (**10**) (796 mg, 81% yield). MS: [M+H] = 246.1 ($C_{14}H_{15}NOS$).

*4.1.5. N-(2,2-diethoxyethyl)-4-iodobenzene-1,2-diamine (**12**)*

Under nitrogen, to a stirred solution of 1-fluoro-4-iodo-2-nitrobenzene (**11**) (30.0 g, 112 mmol, 1.00 equiv) in MeCN (500 mL) at 23 ºC was added 2,2-diethoxyethan-1-amine (14.0 g, 124 mmol, 1.10 equiv) and $^{i}Pr_2NEt$ (43.6 g, 337 mmol, 3.00 equiv). After stirring for 2 hr at 80 ºC, the reaction mixture was concentrated and the residue was diluted with EtOAc. The solution was washed with brine and dried over Na_2SO_4. The filtrate was concentrated in vacuo to afford *N*-(2,2-diethoxyethyl)-4-iodo-2-nitroaniline, which was used in the next step without further purification. MS: [M+H] = 381.0 ($C_{12}H_{18}IN_2O_4$).

Under air, to a stirred solution of *N*-(2,2-diethoxyethyl)-4-iodo-2-nitroaniline (19.0 g, 50.0 mmol, 1.00 equiv) in THF (200 mL) at 0 ºC was added a solution of NH_4Cl (26.7g, 500.0 mmol, 10.0 equiv) in H_2O (40 mL) followed by Zn powder (32.7 g, 500.0 mmol, 10.0 equiv). After stirring for 16 hr at 23 ºC, the reaction mixture was filtered and the filter cake was washed with EtOAc. The combined organic layers were washed with brine and dried over Na_2SO_4. The filtrate was concentrated in vacuo and the residue was purified by column chromatography on silica gel eluting with petroleum ether/EtOAc to afford *N*-(2,2-diethoxyethyl)-4-iodobenzene-1,2-diamine (**12**) (15 g, 87% yield). MS: [M+H] = 351.1 ($C_{12}H_{20}IN_2O_2$).

*4.1.6. 1-(2,2-diethoxyethyl)-5-iodo-1,2,3-benzotriazole (**13**)*

Under air, to a stirred solution of *N*-(2,2-diethoxyethyl)-4-iodobenzene-1,2-diamine (**12**) (16.0 g, 45.7 mmol, 1.00 equiv) in toluene/AcOH (60/48 mL) at 0 ºC was added a solution of $NaNO_2$ (6.3 g, 91 mmol, 2.0 equiv) in H_2O (60 mL) dropwise. After stirring for 1 hr at 0 ºC, the reaction mixture was diluted with EtOAc, washed with brine, and dried over Na_2SO_4. The filatrate was concentrated in vacuo and the residue was purified by column chromatography on silica gel eluting with petroleum ether/EtOAc to afford 1-(2,2-diethoxyethyl)-5-iodo-1,2,3-benzotriazole (**13**) (10 g, 61% yield). MS: [M+H] = 362.0 ($C_{12}H_{17}IN_3O_2$).

*4.1.7. 2-(5-iodo-1H-benzo[d][1,2,3]triazol-1-yl)acetaldehyde (**14**)*

Under air, to a stirred solution of 1-(2,2-diethoxyethyl)-5-iodo-1,2,3-benzotriazole (**13**) (2.0 g, 5.5 mmol, 1.0 equiv) was added HCl (aq) (1.2 M, 40 mL) at 23 ºC. After stirring for 16 hr at 70 ºC, the reaction mixture was cooled to 23 ºC and NaOAc was added in portions to adjusted pH = 6~7. The resulting mixture was extracted with EtOAc and the combined organic layers were dried over Na_2SO_4. The filtrate was concentrated in vacuo to afford 2-(5-iodo-1H-benzo[d][1,2,3]triazol-1-yl)acetaldehyde (**14**), which was used in the next step without further purification. MS: [M+H+H_2O] = 306.0 ($C_8H_9IN_3O_2$).

*4.1.8. N-[2-(5-iodobenzotriazol-1-yl)-1-trimethylsilyloxy-ethyl]-N-tetrahydropyran-2-yloxy-formamide (**15**)*

Under nitrogen, to a stirred solution of *N*-tetrahydropyran-2-yloxyformamide (**7**) (1.89 g, 13.0 mmol, 2.20 equiv) in toluene (51 mL) at 23 ºC was added Et_3N (2.06 mL, 14.8 mmol, 2.50

equiv) and TMSCl (1.88 mL, 14.8 mmol, 2.50 equiv). After stirring for 15 min at 80 ºC, the reaction mixture was cooled to 23 ºC and 2-(5-iodobenzotriazol-1-yl)acetaldehyde (**14**) (1.70 g, 5.92 mmol, 1.00 equiv) was added as a solid. After stirring at 23 ºC for 16 hr, H_2O was added to the reaction mixture and the aqueous layer was extracted with EtOAc. The combined organic layers were washed with H_2O, brine, and dried over $MgSO_4$. The filtrate was concentrated in vacuo and the residue was purified by column chromatography on silica gel eluting with hexanes/EtOAc to afford *N*-[2-(5-iodobenzotriazol-1-yl)-1-trimethylsilyloxy-ethyl]-*N*-tetrahydropyran-2-yloxy-formamide (**15**) (1.5 g, 50% yield). MS: [M+H] = 505.1 ($C_{17}H_{26}IN_4O_4Si$).

*4.1.9. N-hydroxy-N-[2-(5-iodobenzotriazol-1-yl)-1-methylsulfanyl-ethyl]formamide (**16**)*

Under nitrogen, to a stirred solution of *N*-[2-(5-iodobenzotriazol-1-yl)-1-trimethylsilyloxy-ethyl]-*N*-tetrahydropyran-2-yloxy-formamide (**15**) (1.38 g, 2.74 mmol, 1.00 equiv) in CH_2Cl_2 (49 mL) at 23 ºC was added sodium thiomethoxide (2.30 g, 27.4 mmol, 10.0 equiv) and TMSOTf (0.99 mL, 5.5 mmol, 2.0 equiv). After stirring for 10 min at 23 ºC, additional TMSOTf (1.98 mL, 10.9 mmol, 4.00 equiv) was added. After stirring for additional 5 min at 23 ºC, the reaction mixture was diluted with CH_2Cl_2 and sat. $NaHCO_3$ (aq) was added. The organic layer was collected, washed with H_2O, brine, and dried over $MgSO_4$. The filtrate was concentrated in vacuo and the residue was purified by column chromatography on silica gel eluting with hexanes/EtOAc to afford *N*-hydroxy-*N*-[2-(5-iodobenzotriazol-1-yl)-1-methylsulfanyl-ethyl]formamide (**16**) (1.5 g, 87% yield). MS: [M+H] = 379.0 ($C_{10}H_{12}IN_4O_2S$).

*4.1.10. N-hydroxy-N-[1-methylsulfanyl-2-[5-[2-[4-(morpholinomethyl)phenyl]ethynyl]benzotriazol-1-yl]ethyl]formamide (**17**)*

Under nitrogen, to a stirred solution of the literature-known 4-[(4-ethynylphenyl)methyl]morpholine (958 mg, 4.76 mmol, 2.00 equiv) in NMP (15 mL) at 23 ºC was added *N*-hydroxy-*N*-[2-(5-iodobenzotriazol-1-yl)-1-methylsulfanyl-ethyl]formamide (**16**) (900 mg, 2.38 mmol, 1.00 equiv) and degassed by bubbling nitrogen for 10 min. Copper(I) iodide (146 mg, 0.760 mmol, 0.320 equiv), triethylamine (0.66 mL, 4.8 mmol, 2.0 equiv), and $Pd(PPh_3)_4$ (825 mg, 0.710 mmol, 0.300 equiv) were added to the reaction mixture. After stirring for 30 min at 23 ºC, the reaction mixture was concentrated in vacuo and the residue was purified by column chromatography on silica gel eluting with CH_2Cl_2/MeOH to afford *N*-hydroxy-*N*-[1-methylsulfanyl-2-[5-[2-[4-(morpholinomethyl)phenyl]ethynyl]benzotriazol-1-yl]ethyl]formamide (**17**) (545 mg, 46% yield). ^{1}H NMR (300 MHz, DMSO-*d6*, 23 ºC) δ: 10.41 (br s), 9.98 (br s), 8.25 (s, 1H), 8.03 (br s), 7.94 (d, *J* = 8.7 Hz, 1H), 7.88 (br s), 7.70 (d, *J* = 8.7 Hz, 1H), 7.55 (d, *J* = 7.8 Hz, 2H), 7.37 (d, *J* = 7.8 Hz, 2H), 5.92−5.58 (m, 1H), 5.22−5.10 (m, 1H), 5.03−4.94 (m, 1H), 3.61−3.50 (m, 4H), 3.51 (s, 2H), 2.49−2.36 (m, 4H), 2.06 (s, 3H). MS: [M+H] = 452.2 ($C_{23}H_{26}N_5O_3S$).

*4.1.11. N-hydroxy-N-[1-methylsulfanyl-2-[5-[2-[4-[(2-oxo-2λ^4-thia-6-azaspiro[3.3]heptan-6-yl)methyl]phenyl]ethynyl]benzotriazol-1-yl]ethyl]formamide (**18**)*

N-hydroxy-*N*-[1-methylsulfanyl-2-[5-[2-[4-[(2-oxo-2λ^4-thia-6-azaspiro[3.3]heptan-6-yl)methyl]phenyl]ethynyl]benzotriazol-1-yl]ethyl]formamide (**18**) was synthesized in a similar manner as **18**, using compound **10** in place of 4-[(4-ethynylphenyl)methyl]morpholine. ^{1}H NMR

(400 MHz, DMSO-*d*6, 23 ºC) δ: 10.65–9.99 (m, 2H), 8.31 (s, 1H), 8.20–7.85 (m, 2H), 7.79–7.68 (m, 3H), 7.49 (d, *J* = 8.0 Hz, 2H), 5.89–5.66 (m, 1H), 5.22–4.95 (m, 2H), 4.45–3.94 (m, 8H), 3.56 (d, *J* = 11.6 Hz, 2H), 2.12 (d, 3H). MS: [M+H] = 496.1 ($C_{24}H_{26}N_5O_3S_2$).

*4.1.12. N-hydroxy-N-[(1S)-1-methylsulfanyl-2-[5-[2-[4-(morpholinomethyl)phenyl]ethynyl]benzotriazol-1-yl]ethyl]formamide (**19**)*

N-hydroxy-*N*-[(1*S*)-1-methylsulfanyl-2-[5-[2-[4-(morpholinomethyl)phenyl]ethynyl]benzotriazol-1-yl]ethyl]formamide (**19**) was synthesized by chiral HPLC separation of compound **17**. ^{1}H NMR (300 MHz, DMSO-*d6*, 23 ºC) δ: 10.41 (br s), 9.98 (br s), 8.25 (s, 1H), 8.03 (br s), 7.94 (d, *J* = 8.7 Hz, 1H), 7.88 (br s), 7.70 (d, *J* = 8.7 Hz, 1H), 7.55 (d, *J* = 7.8 Hz, 2H), 7.37 (d, *J* = 7.8 Hz, 2H), 5.92−5.58 (m, 1H), 5.22−5.10 (m, 1H), 5.03−4.94 (m, 1H), 3.61−3.50 (m, 4H), 3.51 (s, 2H), 2.49−2.36 (m, 4H), 2.06 (s, 3H). MS: [M+H] = 452.2 ($C_{23}H_{26}N_5O_3S$). Chiral HPLC: column: CHIRALPAK IG-3; column size: 0.46×5 cm, 3 μm; mobile phase: (hexanes: CH_2Cl_2=3:1 with 0.2% isopropylamine)/(EtOH: CH_2Cl_2=1:1)=20/80; flow: 1.0 mL/min; temperature: 25 ºC; RT = 0.91. The absolute stereochemistry was confirmed by X-ray crystallography.

*4.1.13. N-hydroxy-N-[(1S)-1-methylsulfanyl-2-[5-[2-[4-[(2-oxo-2λ4-thia-6-azaspiro[3.3]heptan-6-yl)methyl]phenyl]ethynyl]benzotriazol-1-yl]ethyl]formamide (**20**)*

N-hydroxy-*N*-[(1*S*)-1-methylsulfanyl-2-[5-[2-[4-[(2-oxo-2λ4-thia-6-azaspiro[3.3]heptan-6-yl)methyl]phenyl]ethynyl]benzotriazol-1-yl]ethyl]formamide (**20**) was synthesized by chiral HPLC separation of compound **18**. ^{1}H NMR (400 MHz, DMSO-*d*6, 23 ºC) δ: 10.65–9.99 (m,

2H), 8.31 (s, 1H), 8.20–7.85 (m, 2H), 7.79–7.68 (m, 3H), 7.49 (d, *J* = 8.0 Hz, 2H), 5.89–5.66 (m, 1H), 5.22–4.95 (m, 2H), 4.45–3.94 (m, 8H), 3.56 (d, *J* = 11.6 Hz, 2H), 2.12 (d, 3H). MS: [M+H] = 496.1 ($C_{24}H_{26}N_5O_3S_2$). Chiral HPLC: column: CHIRALPAK IE-3; column size: 0.46×5 cm, 3 μm; mobile phase: MeOH: CH_2Cl_2=1:1; flow: 1.0 mL/min; temperature: 25 ºC; RT = 1.1. The absolute stereochemistry was assumed by comparing biological data with compounds from the same series.

*4.1.14. N-hydroxy-N-(3-(4-((4-(morpholinomethyl)phenyl)ethynyl)phenyl)propyl)formamide (**23**)*

^{1}H NMR (400 MHz, DMSO-*d*6, 23 ºC) δ: 10.01 (s, 0.5H), 9.59 (s, 0.5H), 8.29 (s, 0.5H), 7.90 (s, 0.5H), 7.57–7.26 (m, 8H), 3.58 (br s, 4H), 3.50–3.41 (m, 4H), 2.67 (br s, 2H), 2.18 (br s, 4H), 1.85 (br s, 2H). MS: [M+H] = 379.2 ($C_{23}H_{27}N_2O_3$).

*4.1.15. N-hydroxy-N-(2-(5-((4-(morpholinomethyl)phenyl)ethynyl)-1H-indol-1-yl)ethyl)formamide (**24a**)*

^{1}H NMR (400 MHz, DMSO-*d*6, 23 ºC) δ: 8.18 (s, 0.4H), 7.77 (s, 1H), 7.58–7.29 (m, 7.6H), 6.50–6.45 (m, 1H), 4.42 (br s, 2H), 3.85–3.75 (m, 2H), 3.60 (br s, 4H), 3.41 (s, 2H), 2.37 (br s, 4H). MS: [M+H] = 404.2 ($C_{24}H_{26}N_3O_3$).

*4.1.16. N-hydroxy-N-(2-(5-((4-(morpholinomethyl)phenyl)ethynyl)-1H-benzo[d]imidazol-1-yl)ethyl)formamide (**24b**)*

^{1}H NMR (400 MHz, DMSO-*d*6, 23 ºC) δ: 8.26–8.14 (m, 2H), 7.95–7.80 (m, 1H), 7.70–7.32 (m, 7H), 4.49 (br s, 2H), 3.88 (br s, 2H), 3.66–3.52 (m, 4H), 2.08 (br s, 4H). MS: [M+H] = 405.2 ($C_{23}H_{25}N_4O_3$).

*4.1.17. N-hydroxy-N-(2-(5-((4-(morpholinomethyl)phenyl)ethynyl)-1H-indazol-1-yl)ethyl)formamide (**24c**)*

^{1}H NMR (400 MHz, DMSO-*d*6, 23 ºC) δ: 8.17–7.95 (m, 2H), 7.68–7.30 (m, 7H), 4.59 (br s, 2H), 3.89 (br s, 2H), 3.73 (s, 2H), 3.63 (s, 4H), 2.61 (br s, 4H). MS: [M+H] = 405.2 ($C_{23}H_{25}N_4O_3$).

*4.1.18. N-hydroxy-N-(2-(5-((4-(morpholinomethyl)phenyl)ethynyl)-2-oxoindolin-1-yl)ethyl)formamide (**24d**)*

^{1}H NMR (400 MHz, DMSO-*d*6, 23 ºC) δ: 8.25–8.12 (m, 1H), 7.74 (s, 0.5H), 7.49–7.30 (m, 6.5H), 7.08–7.02 (m, 1H), 3.87 (br s, 2H), 3.71 (br s, 4H), 3.56 (s, 4H), 3.47 (s, 2H), 2.34 (br s, 4H). MS: [M+H] = 420.2 ($C_{24}H_{26}N_3O_4$).

*4.1.19. N-hydroxy-N-(2-(5-((4-(morpholinomethyl)phenyl)ethynyl)-1H-pyrrolo[3,2-b]pyridin-1-yl)ethyl)formamide (**24e**)*

^{1}H NMR (300 MHz, DMSO-*d*6, 23 ºC) δ: 7.87–7.70 (m, 2H), 7.48–7.28 (m, 6H), 6.48 (s, 1H), 4.40–4.21 (m, 2H), 3.52 (br s, 4H), 3.47 (s, 2H), 3.00 (br s, 2H), 2.30 (br s, 4H). MS: [M+H] = 405.2 ($C_{23}H_{25}N_4O_3$).

*4.1.20. N-hydroxy-N-(2-(5-((4-(morpholinomethyl)phenyl)ethynyl)-1H-pyrrolo[2,3-c]pyridin-1-yl)ethyl)formamide (**24f**)*

^{1}H NMR (300 MHz, DMSO-*d*6, 23 ºC) δ: 8.83 (s, 1H), 8.05 (s, 0.4H), 7.77 (s, 1H), 7.55–7.28 (m, 5.6H), 6.46 (br s, 1H), 4.45 (br s, 2H), 3.78 (br s, 2H), 3.52 (br s, 4H), 3.43 (s, 2H), 2.30 (br s, 4H). MS: [M+H] = 405.2 ($C_{23}H_{25}N_4O_3$).

*4.1.21. N-hydroxy-N-(2-(5-((4-(morpholinomethyl)phenyl)ethynyl)-1H-benzo[d][1,2,3]triazol-1-yl)ethyl)formamide (**24g**)*

^{1}H NMR (300 MHz, DMSO-*d*6, 23 ºC) δ: 10.03–9.73 (m, 1H), 8.25 (br s, 1H), 8.10–7.30 (m, 7H), 4.93 (br s, 2H), 4.00 (br s, 2H), 3.58 (br s, 4H), 3.12 (br s, 2H), 2.36 (br s, 4H). MS: [M+H] = 406.2 ($C_{22}H_{24}N_5O_3$).

*4.1.22. N-hydroxy-N-(2-(6-((4-(morpholinomethyl)phenyl)ethynyl)-[1,2,3]triazolo[1,5-a]pyridin-3-yl)ethyl)formamide (**24h**)*

^{1}H NMR (300 MHz, D_2O, 23 ºC) δ: 8.88 (s, 1H), 7.79–7.38 (m, 7H), 3.93 (br s, 4H), 3.81 (br s, 4H), 3.33 (br s, 2H), 2.88 (br s, 4H). MS: [M+H] = 406.2 ($C_{22}H_{24}N_5O_3$).

*4.1.23. N-hydroxy-N-(2-(7-((4-(morpholinomethyl)phenyl)ethynyl)-[1,2,4]triazolo[4,3-a]pyridin-3-yl)ethyl)formamide (**24i**)*

^{1}H NMR (300 MHz, DMSO-*d*6, 23 ºC) δ: 10.20–9.60 (m, 1H), 8.44 (d, J = 7.5 Hz, 1H), 7.97–7.89 (m, 2H), 7.57 (d, J = 8.1 Hz, 2H), 7.40 (d, J = 8.1 Hz, 2H), 7.04 (d, J = 7.5 Hz, 1H), 3.97 (br s, 2H), 3.58–3.30 (m, 8H), 2.88 (br s, 4H). MS: [M+H] = 406.2 ($C_{22}H_{24}N_5O_3$).

*4.1.24. N-hydroxy-N-(1-hydroxy-3-(5-((4-(morpholinomethyl)phenyl)ethynyl)-1H-benzo[d][1,2,3]triazol-1-yl)propan-2-yl)formamide (**25a**)*

^{1}H NMR (400 MHz, DMSO-*d*6, 23 ºC) δ: 10.03–9.73 (m, 1H), 8.25 (br s, 1H), 8.10–7.30 (m, 7H), 4.93–4.77 (m, 4H), 4.00 (br s, 2H), 3.58 (br s, 3H), 3.12 (br s, 2H), 2.36 (br s, 4H). MS: [M+H] = 447.2 ($C_{23}H_{23}N_6O_4$).

*4.1.25. N-hydroxy-N-(1-(5-((4-(morpholinomethyl)phenyl)ethynyl)-1H-benzo[d][1,2,3]triazol-1-yl)propan-2-yl)formamide (**25b**)*

^{1}H NMR (300 MHz, DMSO-*d*6, 23 ºC) δ: 9.99 (br s, 1H), 8.21 (s, 1H), 8.01–7.35 (m, 7H), 5.01–4.72 (m, 2H), 4.40 (br s, 1H), 3.58 (br s, 4H), 3.50 (s, 2H), 2.39 (br s, 4H), 1.40–1.20 (m, 3H). MS: [M+H] = 420.2 ($C_{23}H_{26}N_5O_3$).

*4.1.26. N-hydroxy-N-(1-(5-((4-(morpholinomethyl)phenyl)ethynyl)-1H-benzo[d][1,2,3]triazol-1-yl)butan-2-yl)formamide (**25c**)*

^{1}H NMR (300 MHz, DMSO-*d*6, 23 ºC) δ: 10.00–9.65 (m, 1H), 8.26–7.35 (m, 7H), 5.01–4.12 (m, 3H), 3.58 (br s, 4H), 3.50 (s, 2H), 2.39 (br s, 4H), 1.81–1.50 (m, 2H), 0.90 (t. *J* = 7.2 Hz, 3H). MS: [M+H] = 434.2 ($C_{24}H_{28}N_5O_3$).

*4.1.27. N-(1-(ethylthio)-2-(5-((4-(morpholinomethyl)phenyl)ethynyl)-1H-benzo[d][1,2,3]triazol-1-yl)ethyl)-N-hydroxyformamide (**25d**)*

^{1}H NMR (300 MHz, DMSO-*d6*, 23 ºC) δ: 10.20–9.95 (m, 1H), 8.27 (s, 1H), 8.00 (br s, 1H), 7.94 (d, *J* = 8.7 Hz, 1H), 7.83 (br s, 1H), 7.72 (d, *J* = 8.7 Hz, 1H), 7.55 (d, *J* = 7.8 Hz, 2H), 7.38 (d, *J*

= 7.8 Hz, 2H), 5.92−5.54 (m, 1H), 5.21−5.11 (m, 1H), 5.03−4.96 (m, 1H), 3.61−3.50 (m, 4H), 3.51 (s, 2H), 3.16−3.01 (m, 2H), 2.49−2.35 (m, 4H), 1.19−1.03 (m, 3H). MS: [M+H] = 466.2 ($C_{24}H_{28}N_5O_3S$).

*4.1.28. N-hydroxy-N-(1-methoxy-2-(5-((4-(morpholinomethyl)phenyl)ethynyl)-1H-benzo[d][1,2,3]triazol-1-yl)ethyl)formamide (**25e**)*

^{1}H NMR (300 MHz, DMSO-*d6*, 23 ºC) δ: 10.11 (br s), 9.90 (br s), 8.21 (s, 1H), 8.03 (br s), 7.96 (d, *J* = 8.7 Hz, 1H), 7.91 (br s), 7.71 (d, *J* = 8.7 Hz, 1H), 7.58 (d, *J* = 7.8 Hz, 2H), 7.39 (d, *J* = 7.8 Hz, 2H), 5.92−5.62 (m, 1H), 5.28−5.14 (m, 1H), 5.09−4.91 (m, 1H), 3.61−3.50 (m, 4H), 3.51 (s, 2H), 3.46 (s, 3H), 2.49−2.36 (m, 4H). MS: [M+H] = 436.2 ($C_{23}H_{26}N_5O_4$).

*4.1.29. N-(1-ethoxy-2-(5-((4-(morpholinomethyl)phenyl)ethynyl)-1H-benzo[d][1,2,3]triazol-1-yl)ethyl)-N-hydroxyformamide (**25f**)*

^{1}H NMR (300 MHz, DMSO-*d6*, 23 ºC) δ: 10.04 (br s), 9.80 (br s), 8.11 (s, 1H), 8.13 (br s), 7.99 (d, *J* = 8.7 Hz, 1H), 7.91 (br s), 7.71 (d, *J* = 8.7 Hz, 1H), 7.56 (d, *J* = 7.8 Hz, 2H), 7.35 (d, *J* = 7.8 Hz, 2H), 5.90−5.60 (m, 1H), 5.19−5.04 (m, 1H), 5.00−4.81 (m, 1H), 3.60−3.48 (m, 6H), 3.45 (s, 2H), 2.49−2.36 (m, 4H), 1.12 (t. *J* = 7.2 Hz, 3H). MS: [M+H] = 450.2 ($C_{24}H_{28}N_5O_4$).

*4.1.30. N-hydroxy-N-[(1R)-1-methylsulfanyl-2-[5-[2-[4-(morpholinomethyl)phenyl]ethynyl]benzotriazol-1-yl]ethyl]formamide (**25g**)*

^{1}H NMR (300 MHz, DMSO-*d6*, 23 ºC) δ: 10.41 (br s, 1H), 9.98 (br s, 1H), 8.25 (s, 1H), 8.03 (br s, 1H), 7.94 (d, *J* = 8.7 Hz, 1H), 7.88 (br s), 7.70 (d, *J* = 8.7 Hz, 1H), 7.55 (d, *J* = 7.8 Hz, 2H),

7.37 (d, *J* = 7.8 Hz, 2H), 5.92−5.58 (m, 1H), 5.22−5.10 (m, 1H), 5.03−4.94 (m, 1H), 3.61−3.50 (m, 4H), 3.51 (s, 2H), 2.49−2.36 (m, 4H), 2.06 (s, 3H). MS: [M+H] = 452.2 ($C_{23}H_{26}N_5O_3S$).

*4.1.31. N-(2-(hydroxyamino)-2-oxoethyl)-4-((4-(morpholinomethyl)phenyl)ethynyl)benzamide (**26**)*

^{1}H NMR (400 MHz, DMSO-*d*6, 23 ºC) δ: 10.64 (br s, 1H), 10.37 (br s, 1H), 8.89 (br s, 1H), 7.95 (d, *J* = 8.0 Hz, 2H), 7.72–7.65 (m, 4H), 7.57 (d, *J* = 8.0 Hz, 2H), 4.40 (br s, 2H), 3.96 (br s, 2H), 3.80 (s, 2H), 3.62 (br s, 2H), 3.40–3.02 (m, 4H). MS: [M+H] = 394.2 ($C_{22}H_{24}N_3O_4$).

*4.1.32. N-hydroxy-N-(1-(6-((4-(morpholinomethyl)phenyl)ethynyl)-1H-indazol-3-yl)butan-2-yl)formamide (**27a**)*

^{1}H NMR (300 MHz, $CDCl_3$, 23 ºC) δ: 7.79–7.26 (m, 7H), 4.00–3.07 (m, 9H), 2.61–2.32 (m, 4H), 2.13–1.60 (m, 2H), 1.13–0.92 (m, 3H). MS: [M+H] = 433.2 ($C_{25}H_{29}N_4O_3$).

*4.1.33. N-hydroxy-N-(rac-(3S,4R)-6-hydroxy-4-(6-((4-(morpholinomethyl)phenyl)ethynyl)-1H-indazol-3-yl)heptan-3-yl)formamide (**27b**)*

^{1}H NMR (300 MHz, DMSO-*d*6, 23 ºC) δ: 12.95–12.83 (m, 1H), 9.64–9.09 (m, 1H), 8.15–7.46 (m, 5H), 7.38 (d, *J* = 7.8 Hz, 2H), 7.23–7.13 (m, 1H), 4.52–3.70 (m, 3H), 3.59 (br s, 4H), 3.50 (s, 2H), 2.37 (br s, 4H), 2.12–1.55 (m, 4H), 1.15–0.70 (m, 6H). MS: [M+H] = 491.3 ($C_{28}H_{35}N_4O_4$).

*4.1.34. (S)-N-hydroxy-N-(2-(5-((4-((2-(hydroxymethyl)-1H-imidazol-1-yl)methyl)phenyl)ethynyl)-1H-benzo[d][1,2,3]triazol-1-yl)-1-(methylthio)ethyl)formamide (**28a**)*

^{1}H NMR (400 MHz, Methanol-*d*4, 23 ºC) δ: 8.15–7.79 (m, 3H), 7.70 (d, *J* = 8.7 Hz, 1H), 7.59 (d, *J* = 8.0 Hz, 2H), 7.29 (d, *J* = 8.0 Hz, 2H), 7.16 (s, 1H), 7.01 (s, 1H), 6.00–5.55 (m, 1H), 5.39 (s, 2H), 5.29–5.00 (m, 3H), 4.66 (s, 2H), 2.21 (s, 3H). MS: [M+H] = 463.2 ($C_{23}H_{23}N_6O_3S$).

*4.1.35. (S)-N-(2-(5-((4-(2-oxa-6-azaspiro[3.3]heptan-6-ylmethyl)phenyl)ethynyl)-1H-benzo[d][1,2,3]triazol-1-yl)-1-(methylthio)ethyl)-N-hydroxyformamide (**28b**)*

^{1}H NMR (400 MHz, DMSO-*d*6, 23 ºC) δ: 10.63–9.98 (m, 2H), 8.31 (s, 1H), 8.15–7.85 (m, 2H), 7.79–7.68 (m, 3H), 7.49 (d, *J* = 8.0 Hz, 2H), 5.89–5.66 (m, 1H), 5.22–4.95 (m, 2H), 4.77–4.61 (m, 4H), 4.35 (s, 2H), 4.34–4.21 (m, 4H), 2.12 (d, 3H). MS: [M+H] = 464.2 ($C_{24}H_{26}N_5O_3S$). MS: [M+H] = 450.2 ($C_{24}H_{28}N_5O_4$).

*4.1.36. N-((S)-2-(5-((4-(((3S,4S)-3,4-dihydroxypyrrolidin-1-yl)methyl)phenyl)ethynyl)-1H-benzo[d][1,2,3]triazol-1-yl)-1-(methylthio)ethyl)-N-hydroxyformamide (**28c**)*

^{1}H NMR (400 MHz, DMSO-*d*6, 23 ºC) δ: 8.65–7.70 (m, 4H), 7.55 (d, *J* = 8.0 Hz, 2H), 7.37 (d, *J* = 8.0 Hz, 2H), 5.91–4.91 (m, 2H), 4.82 (s, 2H), 3.85 (br s, 2H), 3.70–3.55 (m, 2H), 2.84–2.75 (m, 2H), 2.40–2.33 (m, 2H), 2.12 (s, 3H). MS: [M+H] = 468.2 ($C_{23}H_{26}N_5O_4S$).

4.1.37. N-*hydroxy*-N-*(2-(5-((4-((2-((methylsulfonyl)methyl)-1*H-*imidazol-1-yl)methyl)phenyl)ethynyl)-1*H-*benzo[*d*][1,2,3]triazol-1-yl)-1-(methylthio)ethyl)formamide (**29**)*

^{1}H NMR (400 MHz, Methanol-*d*4, 23 ºC) δ: 8.23–7.82 (m, 3H), 7.70 (d, *J* = 8.7 Hz, 1H), 7.50 (d, *J* = 8.0 Hz, 2H), 7.23 (d, *J* = 8.0 Hz, 2H), 7.11 (s, 1H), 7.04 (s, 1H), 5.90–5.55 (m, 1H), 5.39 (s, 2H), 5.34–5.00 (m, 3H), 2.21 (s, 3H), 2.81 (s, 3H). MS: [M+H] = 525.1 ($C_{24}H_{25}N_6O_4S_2$).

4.2. Biology

4.2.1. Measurement of inhibitor binding to P. aeruginosa and E. coli LpxC

P. aeruginosa and *E. coli* LpxC proteins were purified as described in Hale et al (2013).[27] The methods for synthesis of the fluorescent ligands **A**, **B** and **C** are described in the Supplementary Material.

Fluorescence anisotropy-based fluorescent ligand displacement assays for measuring IC_{50}s of *P. aeruginosa* LpxC inhibitors used either ligand **A** or **B** in a buffer composed of 50 mM HEPES (pH 7.0) and 0.01% Triton X-100 (Surfact-Amps, Thermo-Fisher Scientific, Waltham, MA). With ligand **A** (K_d = 2.6 nM), assays were performed in low-volume, shallow-well, black polystyrene 384-well plates (Corning Life Sciences, Tewksbury, MA) in a 6 µL volume. Compounds were dissolved at 10 mM in DMSO. Two-fold serial dilutions were prepared in buffer from 10 µM to 9.8 nM, and a 0 µM sample was included. To each of 6 wells was added 3 µL of each inhibitor concentration. To 3 of the wells was added 3 µL of 2 nM ligand **A**. To the

remaining 3 wells was added 3 µL of a mixture containing 2 nM ligand **A** and 4 nM *P. aeruginosa* LpxC.

With ligand **B** (K_d = 0.32 nM), the assay was performed in standard 384-well black polystyrene plates (Greiner Bio-One, Monroe, NC) in a 54 µL volume. Two-fold serial dilutions of inhibitor were prepared in buffer from 3 µM to 2.93 nM, and a 0 µM sample was included. In addition, to provide a value for 100% inhibition, samples were prepared containing 3 µM compound **29** (structure shown in Fig. 6) (IC_{50} = 1 nM). To each of 3 wells was added 18 µL of each inhibitor concentration, 18 µL of 600 pM ligand **B**, and 18 µL of 1.2 nM *P. aeruginosa* LpxC.

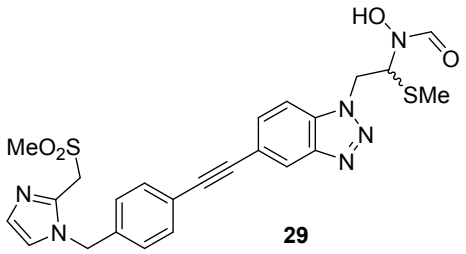

29

Fig. 6. Structure of compound **29**

IC_{50}s measured with ligands **A** and **B** resulted in indistinguishable IC_{50}s. Ligand **B** was used to extend the low end of the range of potency measurements 5-fold below those that were possible with ligand **A** by reducing the final *P. aeruginosa* LpxC concentration from 2 nM to 400 pM. IC_{50}s of *E. coli* LpxC inhibitors used ligand C (K_d = 7.4 nM) in a buffer composed of 50 mM HEPES (pH 8.0), 0.01% Triton X-100, 0.5 M sucrose, 200 µM dithiothreitol, and 10 µM EDTA. Assays of 6 µL volume were performed in low-volume, shallow-well, black polystyrene 384-well plates. Compounds were dissolved at 10 mM in DMSO. Two-fold serial dilutions were prepared in buffer from 10 µM to 0.98 µM, and a 0 µM sample was included. To each of 6 wells

was added 3 μL of each inhibitor concentration. To 3 of the wells was added 3 μL of 2 nM ligand **C**. To the remaining 3 wells was added 3 μL of a mixture containing 2 nM ligand **C** and 12.5 nM *E. coli* LpxC.

After incubation at ambient temperature for 30 min, the fluorescence anisotropy of the ligand was measured with a Pherastar FS plate reader (BMG Labtech, Cary, NC) using a fluorescence polarization optics module containing 540 nm excitation and 590 nm emission filters with either 100 or 200 flashes/well.

The % inhibition was calculated for each competitor concentration according to Eqn. 1,

Eqn. 1. $$\% \text{ inhibition} = 100 \times [1 - (X - MIN)/(MAX - MIN)]$$

where X is the anisotropy measurement in the presence of the competitor, MIN is the anisotropy at 100% competition (with ligand **B**) or in the absence of LpxC (with ligands **A** and **C**), and MAX is the anisotropy in the absence of competitor.

The IC_{50} was calculated by nonlinear regression of the set of % inhibition versus inhibitor concentration values using Eqn. 2,

Eqn. 2. $$\% \text{ inhibition} = MAX\%[I]^n/(IC_{50}^n + [I]^n)$$

where MAX% is the maximal % inhibition achieved at inhibitor saturation (typically ~100%), [I] is the inhibitor concentration, and n is the Hill slope of the curve.

When inhibitor concentrations are relatively high, interference by the inhibitors with fluorescence intensity and/or anisotropy measurements may be significant, such as by compound fluorescence, quenching of probe fluorescence, inner filter effect, or light scattering from solids. In such cases, with ligands **A** and **C**, the method of artifact correction described by Shapiro et al (2009) was employed.[28]

4.2.2. Antibacterial activity against Gram-negative clinical isolates

The minimal inhibitory concentration (MIC) values of compounds against *P. aeruginosa, E. coli* and *K. pneumoniae* were determined using the Clinical and Laboratory Standards Institute guidelines (CLSI) broth microdilution methodology.[29]

4.2.3. X-ray crystallography

Crystallization: A 100 mM DMSO stock solution of compound **19** was added to the LpxC protein to a final concentration of 2 mM and incubated overnight at 4 ºC. The LpxC + **19** solution was cleared by centrifugation to remove precipitation at 13000 × g for 1 minute and diluted to 5 mg/mL with protein buffer (20 mM HEPES 7.0, 200 mM NaCl). Crystals were obtained by mixing the protein in a 1:1 ratio with reservoir solution (1.6 M $(NH_4)_2SO_4$, 0.5 M LiCl) in a hanging drop apparatus. Fully grown crystals were transferred to a cryoprotectant solution of 1.6 M $(NH_4)_2SO_4$, 0.5 M LiCl, and 20% glycerol before being flash frozen in liquid nitrogen.

X-ray data collection and processing: X-ray diffraction data for LpxC + **19** were collected on the SBC 19-ID beamline at the Advanced Photon Source (APS) in Argonne, IL, and processed with

the HKL3000 software suite.[30] The CCP4 version of MOLREP was used for molecular replacement using a previously solved LpxC (PDB code: 5U39) as a reference model.[9] Rigid and restrained refinements were performed using REFMAC and model building with COOT.[31,32]

4.2.4. In vivo efficacy study

Animals: Female CD-1 mice from Charles River Laboratories and were allowed to acclimate for 5 days prior to start of study. Animals were housed 3 per cage with free access to food and water. Mice received two doses of cyclophosphamide on days -4 and -1 with 150 mg/kg and 100 mg/kg delivered IP, respectively. All procedures were performed to NeoSome IACUC policies and guidelines as well as OLAW standards.

Inoculum Preparation: *E. coli* strain ARC 6599, was prepared for infection from an overnight plate culture. A portion of the plate was resuspended in sterile saline and adjusted to an OD of 0.13 at 625 nm. The adjusted bacterial suspension was further diluted to target an infecting inoculum of 1.0×10^6 CFU/mouse. Plate counts of the inoculum were performed to confirm inoculum concentration. The actual inoculum input was 7.6×10^5 CFU/mouse thigh.

Infection: Mice were inoculated with 100 μL of the prepared bacterial suspension via intramuscular injection into both rear thighs.

Test Agent formulation: Compound **19** was prepared by initially dissolving in DMSO at 5% of the total calculated volume. Once the powder was in solution, vehicle component A3DD (2.5% Dextrose 20 mM Acetate Buffer) was added in a volume to achieve the final volume. The solution was sonicated and vortexed until fully dissolved. The pH of the formulated compound was 3.0. Levofloxacin was prepared in sterile water for injection.

Efficacy: Beginning at two hours post infection mice were dosed with either test articles, positive control antibiotic, or vehicle. Mice receiving test agent or vehicle were dosed subcutaneously or orally at 20 mL/kg. Three animals were dosed per group per dose concentration. Three mice were euthanized at initiation of therapy (T-Rx) and CFUs determined. All remaining mice were euthanized at 26 hours post infection. At termination, thighs were aseptically excised, weighed, and homogenized to a uniform consistency in 2 mL of sterile saline. The homogenates were serially diluted and plated on bacterial growth media. The CFUs were enumerated after overnight incubation. The average and standard deviation for each group were calculated, based on log(CFU).

4.2.5. Measurement of inhibitor binding to AChE

Purified, recombinant human acetylcholinesterase expressed in HEK293 cells, acetylthiocholine substrate, and Ellman's reagent [5,5-dithio-bis-(2-nitrobenzoic acid)] for thiol detection were from Millipore-Sigma. The assay was performed in buffer composed of 0.1 M sodium phosphate (pH 7.4) and 0.01% Triton X-100. Test compounds were dissolved in DMSO at 10 mM. Two-fold serial dilutions of compounds from 300 μM to 0.29 μM, plus 0 μM, were prepared in assay buffer supplemented with 3% (v/v) DMSO to maintain a constant DMSO concentration of 3% (v/v) in the dilutions. Ten μL of the dilutions were added to 2 wells of a clear polystyrene 384-well assay plate, followed by 10 μL of solution consisting of 1.2 mM each of Ellman's reagent and acetylthiocholine in assay buffer. As a blank, 10 μL of buffer was added to one of the duplicate wells. The reactions were initiated by addition to the other duplicate well of 10 μL of 0.006 U/mL acetylcholinesterase. The absorbance at 412 nm was monitored at 1-min intervals

for 1 hour with a Spectramax Plus 384 plate reader (Molecular Devices, San Jose, CA). The blanks were subtracted, and the slopes of the progress curves were measured. The % inhibition values were calculated based on the slope measurements with Eqn. 1, with MIN = 0. IC_{50}s were calculated using equation 2.

4.2.6. Plasma protein binding measurement

Plasma protein binding was measured by a rapid equilibrium dialysis (RED) assay described below.

Plasma was spiked with compound to give the final compound concentration of 5 μM. Spiked plasma (300 μL) was placed in the sample chambers, and the buffer chambers were filled with 500 μL of PBS. The plates were then covered with adhesive seals and incubated at 37 ºC for 7 hr on an orbital shaker set at 400 rpm. Following incubation, samples were removed from both chambers and processed by protein precipitation with crash solution (acetonitrile containing 0.1% formic acid and 250 ng/mL carbutamide as internal standard), followed by vortexing and centrifugation prior to loading the supernatant on LC-MS/MS for quantification. The LC-MS/MS peak area ratio of the test material to the peak area of the internal standard was used to calculate the fraction unbound (fu). The fraction unbound (fu) in plasma was calculated as the ratio between the peak area ratio in the buffer chamber and the peak area ratio in the sample chamber (Eqn. 3). The recovery for each assay was calculated using equation 4 and was considered acceptable between 70 and 130%.

Eqn. 3. fraction unbound (fu) =

peak area ratio in buffer chamber/peak area ratio in sample chamber

Eqn. 4. recovery (%) = 100 ×

(peak area ratio in buffer chamber × 0.5 + peak area ratio in plasma sample chamber × 0.3)/

(peak area ratio in sample chamber (at t = 0) × 0.3)

4.2.7. Rat pharmacokinetics study

Animals: Male Sprague-Dawley rats were received from Charles River laboratories and acclimated for at least 5 days prior to the start of the study. The rats had free access to food and water except for an overnight fast prior to dosing. The animals were housed 1 per cage in a temperature- and humidity-controlled room with a 12-hour light cycle.

Design: Compound **19** was formulated at 90 mg/mL in A5D (2.5% dextrose in 20 mm acetate buffer, pH 5). Rats received a single IV bolus dose of the formulated test article via slow push in the tail vein. Dose volume was adjusted based on body weight (1 mL/kg). Blood samples were collected at selected time points via saphenous venipuncture. The collected blood samples were placed in K_2EDTA micro-tubes for plasma separation.

4.2.8. Rat hemodynamic assay

Male Sprague-Dawley rats were anesthetized using ~2% isoflurane in oxygen and indwelling catheters surgically placed in the femoral artery, femoral vein, and jugular vein for blood pressure measurement, intravenous infusion of test article, and blood sampling, respectively.

Body temperature was maintained using heating pads supplemented with heat lamps if required. Animals were maintained on isoflurane (~1.5% in oxygen) throughout data collection. Animals received vehicle at 10 mL/kg/hr intravenously over 30 min followed by 60-min infusions of test article (Group 1) or vehicle (Group 2) at 10 mL/kg/hr. Both groups were subsequently dosed with additional 30-min infusions of vehicle at 10 mL/kg/hr.

Blood samples (~250 μL) were collected into K_3EDTA tubes at the end of each infusion period, rendered to plasma, and stored at −80 ºC. Animals were euthanized following the final data and blood collection period. Mean arterial pressure (MAP), systolic and diastolic blood pressure (SBP, DBP), and heart rate (HR) were measured and expressed as minute averages over the study duration.

Declaration of Competing Interest

The authors declare the following competing financial interest(s): All authors, except Michael D. Sacco and Yu Chen, are current or former employees of Entasis Therapeutics and may own stock or stock options from Entasis Therapeutics.

Acknowledgments

The authors thank Pharmaron for their synthetic support. They also thank Neosome and Michigan State University for pharmacology support. They also thank the staff members of the Advanced Photon Source of Argonne National Laboratory, particularly those at the Structural Biology Center (SBC), for assistance with X-ray diffraction data collection. SBC-CAT is operated by UChicago Argonne, LLC, for the U.S. Department of Energy, Office of Biological

and Environmental Research under contract DE-AC02-06CH11357. This work was supported, in part, by the Office of the Assistant Secretary of Defense for Health Affairs, through the Combating Antibiotic-Resistant Bacteria Program under Award No. W81XWH-17-2-0004. The U.S. Army Medical Research Acquisition Activity, 820 Chandler Street, Fort Detrick MD 21702-5014 is the awarding and administering acquisition office. In conducting research using animals, they adhered to the laws of the United States and regulations of the Department of Agriculture. Opinions, interpretations, conclusions and recommendations are those of the authors and are not necessarily endorsed by the Department of Defense.

Appendix A. Supplementary Material

Supplementary data to this article can be found online at https://.....

References

1. Theuretzbacher U, Outterson K, Engel A, Karlén A. The global preclinical antibacterial pipeline. *Nat Rev Microbiol*. 2020;18(5):275–285. doi:10.1038/s41579-019-0288-0
2. Williams AH, Raetz CRH. Structural basis for the acyl chain selectivity and mechanism of UDP-N-acetylglucosamine acyltransferase. *Proc Natl Acad Sci U S A*. 2007;104(34):13543–13550. doi:10.1073/pnas.0705833104
3. Erwin AL. Antibacterial drug discovery targeting the lipopolysaccharide biosynthetic enzyme LpxC. *Cold Spring Harb Perspect Med*. 2016;6(7). doi:10.1101/cshperspect.a025304
4. Jackman JE, Fierke CA, Tumey LN, et al. Antibacterial agents that target lipid A

biosynthesis in gram-negative bacteria. Inhibition of diverse UDP-3-O-(R-3-hydroxymyristoyl)-*N*-acetylglucosamine deacetylases by substrate analogs containing zinc binding motifs. *J Biol Chem*. 2000;275(15):11002–11009. doi:10.1074/jbc.275.15.11002

5. Clements JM, Coignard F, Johnson I, et al. Antibacterial activities and characterization of novel inhibitors of LpxC. *Antimicrob Agents Chemother*. 2002;46(6):1793–1799. doi:10.1128/AAC.46.6.1793-1799.2002
6. McClerren AL, Endsley S, Bowman JL, et al. A slow, tight-binding inhibitor of the zinc-dependent deacetylase LpxC of lipid a biosynthesis with antibiotic activity comparable to ciprofloxacin. *Biochemistry*. 2005;44(50):16574–16583. doi:10.1021/bi0518186
7. Montgomery JI, Brown MF, Reilly U, et al. Pyridone methylsulfone hydroxamate LpxC inhibitors for the treatment of serious Gram-negative infections. *J Med Chem*. 2012;55(4):1662–1670. doi:10.1021/jm2014875
8. Brown MF, Reilly U, Abramite JA, et al. Potent inhibitors of LpxC for the treatment of gram-negative infections. *J Med Chem*. 2012;55(2):914–923. doi:10.1021/jm2014748
9. Piizzi G, Parker DT, Peng Y, et al. Design, synthesis, and properties of a potent inhibitor of *Pseudomonas aeruginosa* deacetylase LpxC. *J Med Chem*. 2017;60(12):5002–5014. doi:10.1021/acs.jmedchem.7b00377
10. Zhang J, Chan A, Lippa B, et al. Structure-based discovery of LpxC inhibitors. *Bioorganic Med Chem Lett*. 2017;27(8):1670–1680. doi:10.1016/j.bmcl.2017.03.006
11. Surivet JP, Panchaud P, Specklin JL, et al. Discovery of novel inhibitors of LpxC displaying potent *in vitro* activity against Gram-negative bacteria. *J Med Chem*. 2020;63(1):66–87. doi:10.1021/acs.jmedchem.9b01604

12. Onishi HR, Pelak BA, Gerckens LS, et al. Antibacterial agents that inhibit lipid A biosynthesis. *Science*. 1996;274(5289):980–982. doi: 10.1126/science.274.5289.980

13. US SEC, Form S-1, Achaogen, Inc. www.sec.gov/Archives/edgar/data/1301501/000119312514020548/d623715ds1.htm Accessed 18 September 2020.

14. US National Library of Medicine. ClinicalTrials.gov. https://clinicaltrials.gov/ct2/show/NCT03832517 Accessed 18 September 2020.

15. Cohen F, Aggen JB, Andrews LD, et al. Optimization of LpxC inhibitors for antibacterial activity and cardiovascular safety. *ChemMedChem*. 2019;14(16):1560–1572. doi:10.1002/cmdc.201900287

16. Dalvie D, Cosker T, Boyden T, et al. Metabolism distribution and excretion of a matrix metalloproteinase-13 inhibitor, 4-[4-(4-fluorophenoxy)-benzenesulfonylamino]tetrahydropyran-4-carboxylic acid hydroxyamide (CP-544439), in rats and dogs: assessment of the metabolic profile of CP-544439 in plasma and urine of humans. *Pharmacology*. 2008;36(9):1869–1883. doi:10.1124/dmd.108.022566

17. Sixto-López Y, Gómez-Vidal JA, de Pedro N, et al. Hydroxamic acid derivatives as HDAC1, HDAC6 and HDAC8 inhibitors with antiproliferative activity in cancer cell lines. *Sci Rep*. 2020;10(1):1–17. doi:10.1038/s41598-020-67112-4

18. Lee MS, Isobe M. Metabolic activation of the potent mutagen, 2-naphthohydroxamic acid, in *Salmonella typhimurium* TA98. *Cancer Res*. 1990;50(14):4300–4307.

19. Révész L, Schlapbach A, Wälchl R. Pyrrolo isoquinolines as kinase inhibitors.

WO2008025512A1. 2008.

20. Johnson AP, Luke RWA, Steele RW, et al. Synthesis of 1-acylamino-1-(trimethylsiloxy)alkanes by trimethylsilyl trifluoromethanesulfonate-catalysed addition of bis(trimethylsilyl)amides to aldehydes. *J Chem Soc - Perkin Trans 1*. 1996;(9):883–893. doi:10.1039/p19960000883

21. Johnson AP, Luke RWA, Boa AN. Reactions of 1-acylamino-1-(trimethylsi1oxy)alkanes: versatile precursors to acylimines. *J Chem Soc - Perkin Trans 1*. 1996;(9):895–905. doi:10.1039/p19960000895

22. Mansoora UF, Vitharanaa D, Reddya PA, et al. Design and synthesis of potent Gram-negative specific LpxC inhibitors. *Bioorg Med Chem Lett.* 2011;21(4):1155–1161. doi.org/10.1016/j.bmcl.2010.12.111

23. Cavalli A, Poluzzi E, De Ponti F, et al. Toward a pharmacophore for drugs inducing the long QT syndrome: insights from a CoMFA study of HERG K^+ channel blockers. *J. Med. Chem.* 2002;45(18), 3844–3853. doi.org/10.1021/jm0208875

24. Finch H, Van Niel BM, Woo C. Derivatives of 4-hydroxy-1,2,3,4-tetrahydronaphtalen-1-yl urea and their use in the treatment of, inter alia, diseases of the respiratory tract. WO2013083206A1. 2013.

25. Kim JH, Gensch T, Zhao D, et al. Rh^{III}-catalyzed C−H activation with pyridotriazoles: direct access to fluorophores for metal-ion detection. *Angew Chem Int Ed*. 2015;54(37):10975–10979. doi.org/10.1002/anie.201504757

26. Anderson NH, Bowman J, Erwin A, et al. Antibacterial agents. WO2004062601A2. 2004.

27. Hale MR, Hill P, Lahiri S, et al. Exploring the UDP pocket of LpxC through amino acid

analogs. *Bioorganic Med Chem Lett*. 2013;23(8):2362–2367. doi:10.1016/j.bmcl.2013.02.055

28. Shapiro AB, Walkup GK, Keating TA. Correction for interference by test samples in high-throughput assays. *J Biomol Screen*. 2009;14(8):1008–1016. doi:10.1177/1087057109341768

29. Weinstein MP, Limbago B, Patel JB, et al. Methods for dilution antimicrobial susceptibility tests for bacteria that grow aerobically; approved standard. *Clinical and Laboratory Standards Institute.* Document M07-A11. Wayne, PA, USA; 2018.

30. Minor W, Cymborowski M, Otwinowski Z, et al. *HKL-3000*: the integration of data reduction and structure solution–from diffraction images to an initial model in minutes. *Acta Cryst.* 2006;D62:859–866. doi.org/10.1107/S0907444906019949

31. Murshudov GN, Skubák P, Lebedev AA, et al. *REFMAC5* for the refinement of macromolecular crystal structures. *Acta Cryst.* 2011;D67:355–367. doi.org/10.1107/S0907444911001314

32. Emsley P, Cowtan K. *Coot*: model-building tools for molecular graphics. *Acta Cryst.* 2004;D60:2126–2132. doi.org/10.1107/S0907444904019158

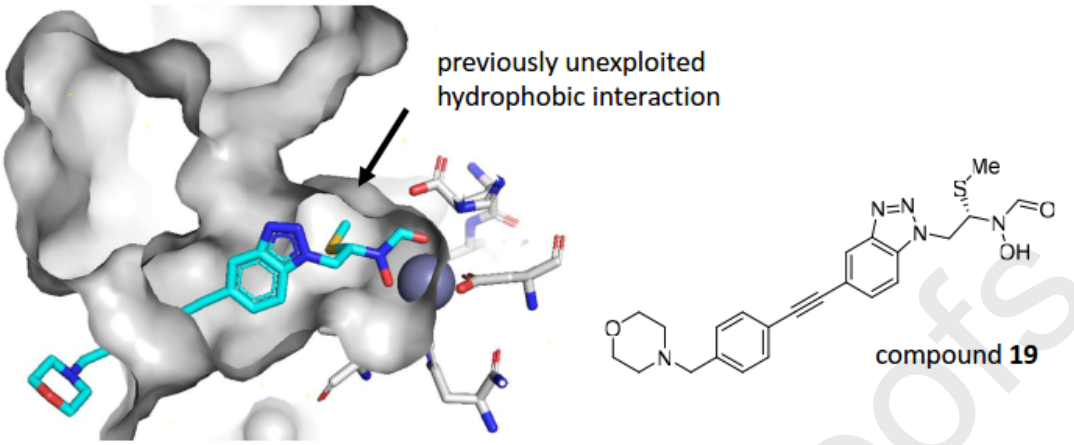

- *New chemotype with N-hydroxyformamide warhead and thioaminal*
- *Unprecedented exploitation of unique binding pocket*
- *Evaluation of in vivo efficacy and safety*

Declaration of interests

☐ The authors declare that they have no known competing financial interests or personal relationships that could have appeared to influence the work reported in this paper.

☒The authors declare the following financial interests/personal relationships which may be considered as potential competing interests:

All authors, except Michael D. Sacco and Yu Chen, are current or former employees of Entasis Therapeutics and may own stock or stock options from Entasis Therapeutics.